9-23-2015 12:00 AM

Application of 3D Printing Technology in Porous Anode Fabrication for Enhanced Power Output of Microbial Fuel Cells

Bin Bian, *The University of Western Ontario*

Supervisor: Jun Yang, *The University of Western Ontario*
A thesis submitted in partial fulfillment of the requirements for the Master of Engineering
Science degree in Mechanical and Materials Engineering
© Bin Bian 2015

Recommended Citation

APPLICATION OF 3D PRINTING TECHNOLOGY IN POROUS ANODE
FABRICATION FOR ENHANCED POWER OUTPUT OF MICROBIAL FUEL CELLS

(Thesis format: Monograph)

by

Bin <u>Bian</u>

Graduate Program in Mechanical and Materials Engineering
Faculty of Engineering

A thesis submitted in partial fulfillment
of the requirements for the degree of
Master of Engineering Science

The School of Graduate and Postdoctoral Studies
The University of Western Ontario
London, Ontario, Canada

Abstract

Microbial fuel cells (MFCs) are widely researched for application in wastewater treatment. However, the current anodes used in MFCs often suffer from high fabrication cost and uncontrollable pore sizes. In this thesis, three-dimensional printing technique was utilized to fabricate anodes with different micro pore sizes for MFCs. Copper coating and carbonization were applied to the printed polymer anodes to increase the conductivity and specific surface area. Voltages of MFCs with various anodes were measured as well as other electrochemical tests such as linear sweep voltammetry and electrochemical impedance spectroscopy. 3D copper porous anode produced higher maximum voltages and power densities compared to copper mesh anode, illustrating the advantage of 3D porous structures in MFC application. However, due to copper corrosion, copper anodes presented much lower power output than carbon cloth anode. As carbon materials are known for their chemical stability, relatively good conductivity and excellent biocompatibility, MFCs with 3D carbon porous anodes were thus developed via carbonization, with larger surface area, higher electricity output, lower diffusion resistance and more bacterial biofilm formation compared to carbon cloth anode. This research project is the first application of 3D printing in MFCs and has developed several simple methods of 3D porous anode fabrication.

Keywords

Acknowledgments

Completion of this thesis work is the result of not only my efforts but also help from other people who offered me great assistance and encouragement during my master study. I would like to express my sincere thanks to them.

First of all, I would like to thank my supervisor, Dr. Jun Yang. I still remember the day when he introduced me to this exciting and brand new research project and gave me total freedom to do research. Prof. Yang is always supportive and ready to offer help when necessary. His valuable ideas and suggestions have motivated me to get new insights into several research topics and broadened my horizon.

I also would like to thank Prof. Andy Sun, from whom I learnt lots of knowledge about fuel cells. Taking his Fuel Cell and Nanomaterials & Nanotechnology courses and doing EIS measurement in his lab are very good experience for me. I must also think Ms. Xia Li and Mr. Wei Xiao, who always assisted me in EIS measurement and fuel cell problem solving.

My thanks also go to Dr. James J. Noël and Ms. Nazhen Liu in Chemistry department for their generous help with the EIS data fitting and testing. Technical support from Surface Science Western, Mr. Brad Kobe and Ms. Rebecca Jacklin, are highly appreciated. They provided great support during the research and taught me how to use SEM to do morphology characterization.

I would also like to appreciate the assistance from the following colleagues: Dr. Mingjun Hu, Dr. Qiuquan Guo, Dr. Xiaobing Cai, Mr. Dongxing Zhang, Mr. Junfeng Xiao, Mr. Luyang Zhang and Mr. Zhaoliang Yang. Dr. Hu offered great assistance in copper electroless coating

and Dr. Cai gave me lots of guidance of carbonization of polymers. They were very supportive during my research, I owe them tremendous gratitude.

Finally, I would like to express my sincere gratitude to my family, especially my father and my grandma. Thanks a lot for your consistent trust and support. It would not have been possible without you.

Table of Contents

List of Tables

List of Figures

List of Appendices

Chapter 1

1   Introduction

In this chapter, the background of this thesis work will be briefly introduced. Also presented here are the research goal and the outline of this thesis.

1.1   Brief Background

Due to the shortage of fossil fuels and the environmental pollution caused during fossil fuel mining and usage, renewable energy and clean water have drawn attention around the world. Researchers have been making lots of efforts to find alternate energy that is reliable and clean, however no such energy has been discovered to totally replace the fossil fuels. In this situation, we may only utilize various energy sources for different applications. And according to World Water Council, about 60% of the world's population will reside in urban areas by 2030. The high population density will create a dramatically increasing demand for energy and water.[1] In fact, water resources and energy production are interdependent as energy is always needed to do wastewater treatment and water is required by hydroelectric power station to provide cheap energy. Bruce E. Logan has estimated that 4-5% of electricity in the US is produced for water infrastructures and about 1.5% of electricity goes directly to wastewater treatment alone.[2] Reducing the energy consumption of wastewater treatment plants can be a big step in constructing sustainable society. Though there hasn't been any technical breakthrough that enables us to solve all the challenges faced by human, many technologies together can help people address certain problems and thus live a life of quality in a sustainable

manner. Microbial fuel cells (MFCs) are such kind of technology that can do wastewater treatment and at the same time produce energy.

Microbial fuel cells (MFCs) are innovative power output devices, which utilize microorganisms as catalysts to metabolize organisms in wastewater and convert chemical energy into electrical energy. Bacteria on the anode oxidize organic compounds anaerobically producing electrons, protons and CO_2. Electrons are then transferred through the external circuit from the anode to the cathode, where electrons together with protons diffused from the anode and oxygen (or other electron acceptors) form water. As there is no byproduct other than H_2O and CO_2, and lots of organisms exist in wastewater, MFCs are ideal devices that can be used to possess both waste disposal in wastewater and electricity output at the same time.

Electron transfer onto anode surface is the key step during the whole electricity-generating process of MFC. The intrinsic properties of anode materials directly affect bacterial adhesion and electron transfer. Therefore, it is quite important to choose proper anode materials in order to improve MFC performance. The essential requirements for anode materials include high conductivity, high specific surface area, high porosity, non-corrosiveness, non-bacteria clogging, good compatibility and low cost. However, porous electrodes recently reported had either large (>500 μm)[3,4] or small (<10 μm)[5] pore sizes which were hard to be tuned. The performance of porous anodes is greatly affected by the pore size of matrix, in which a too large or too small pore size may not be ideal for bacteria growth. Xie et al[6] reported that porous materials with pore sizes less than 10 μm were easily clogged by bacterial growth and hindered the mass transfer into the electrode interior, which wasted the surface area. Besides, there haven't been any articles published

on specific anode pore sizes which were best for bacterial growth in microbial fuel cells. This inspires me to further explore the impacts of pore sizes and surface area of anode materials on MFC performance and discover an alternative method to fabricate anodes with good conductivity, proper pore sizes and low cost. 3D printing technology, because of its advantage in rapid and precise structure fabrication, has drawn lots of interest from engineers and scientists. As researchers in our lab has reported several 3D structures with precisely controllable pore sizes, ranging from $25\,\mu m$ to several hundred microns, and various surface functions[7,8], we believe we could improve the performance of MFCs by preparing 3D anodes with pore sizes that are suitable for bacterial growth.

1.2 Research Goal and Outline of this Thesis

The goal of this thesis work is to explore how 3D printing technique, along with electroless metal plating and carbonization, can be utilized to fabricate MFC anodes with controllable porosity, good conductivity and low cost. To achieve this goal, Shewanella oneidensis strain MR-1 is inoculated into MFCs with 3D printed anodes to degrade the organism and to study the impacts of porous anodes on MFC performances. MR-1 was chosen because it has been reported[9] that this kind of bacteria were able to produce bacterial nanowires, which could help transfer the electrons to anode materials in MFCs. The electrochemical, electrical and biocompatible properties of the 3D printed anodes are studied using techniques including LabVIEW programming, micro fabrication, voltage measurement, linear sweep voltammetry (LSV), electrochemical impedance spectroscopy (EIS) and scanning electron microscope (SEM).

Chapter 2 presents a detailed review of the development of MFC technology and the currently known anode materials used in MFC devices, including carbon-based materials, metal and conductive polymers. As there are some limitations of the traditional anode fabrication process, 3D printing technique is introduced, due to its capability of printing structures with high precision, as well as three kinds of most common 3D printing systems. Its rapid application in personal customization, automobile industry and model fabrication, allows one to create sophisticated and low-cost devices of high precision.

In Chapter 3, a brief introduction to metal electroless plating is provided. Detailed anode fabrication process by 3D printing and electroless copper plating of anode structures are also described. Besides, MR-1 cultivation and inoculation are discussed as well as MFC construction in this chapter. In addition, voltage measurement and LSV are presented to study the impacts of 3D structures on MFC performance. Inductively coupled plasma mass spectrometry (ICP-MS), energy-dispersive X-ray (EDX) and biofilm characterization on 3D printed copper anodes by SEM are conducted to research the corrosion of copper coating on anode surface.

Chapter 4 starts with a short introduction to polymer carbonization. Also presented here is the fabrication process of 3D anodes with different pore sizes. Carbonization of these anodes is introduced to achieve high conductivity. Again, voltage measurement, LSV and biofilm formation are discussed to find out which pore size is best for bacteria growth on anodes. EIS is also measured to determine the internal resistance of different anode structures. All 3D printed porous anodes are found to show better performance compared with MFC with carbon cloth anode.

Chapter 5 gives the summary of this thesis, the contribution part and some suggestions for future work.

Most of the work presented in this thesis has been published in peer-reviewed journals or submitted for publication.

Chapter 2

2 Literature Review

In this chapter, the development of MFC technology and anode materials used in MFC is reviewed. The basic mechanism of bioenergy generation is always reduction and oxidation reactions involving electron transfer within cells and outside of the cells to terminal electron acceptors (extracellular electron transfer). However, what really decides the amount of electricity output is the electron transfer to the anodes. There have been pretty much research on bacteria electron mechanism and anode fabrication, but how to make MFC anodes with low cost, high surface area and high conductivity is yet a tough problem which requires more exploration. 3D printing technology, due to its advantage in fabricating sophisticated and low-cost devices, has drawn lots of attention from both research and industry. Three main printing methods are reviewed here along with the various applications of 3D printing.

2.1 Microbial Fuel Cells

2.1.1 Research background

Microbial fuel cells are new devices that can convert chemical energy into electricity. Utilizing microorganisms as catalysts, MFCs could generate electricity by degrading organism, making a win-win solution for both waste disposal and energy production, and are an ideal technique for future wastewater treatment industry.

In fact, MFC model has been established since Year 1911. British botanist M.C. Potter[10] found that current could be produced by cultivation of E. coli in glucose medium anaerobically. This was the first MFC model which utilized bacteria metabolism to

produce an open circuit voltage of 0.3~0.5V and a current of 0.2 mA at that time. But no significant progress was achieved during the following 55 years after that. Not until 1990s, researchers began to pay attention to microbial fuel cells due to the hot enthusiasm of fuel cell research.[11] Recent report on bacteria Geobacter sulfurreducens KN400 in MFCs drove more researchers to envisage MFC technology as this kind of bacteria could help produce large currents in MFC systems and was named one of 50 most significant discoveries in 2009 by Time magazine.[12]

Microbial fuel cells have several advantages compared with other fuel cells:

1) Fuel sources. Fuel of microbial fuel cells can be various organisms including glucose, lactate, daily wastewater, starch, wastewater from beer factory and even the phenol, which is very hard to be degraded.

2) Easy operation and no further pollution. Microbial fuel cells can be operated at room temperatures with no other requirement for air pressure or locations. Organisms are oxidized without the acidification of water as the only products of MFCs are H_2O and CO_2.

3) Long life circle. Microorganisms are known to have various kinds of oxidoreductases, which can be used for fuel oxidization. As enzymes are reproducible in bacteria, MFCs can run for quite a long time given enough nutrition. MFCs operated for more than 5 years have been reported so far. [13,14]

So far, MFCs have shown great potential in wastewater treatment. This technique is different from other wastewater treatment methods as there is no need for external energy supplied to MFC systems. Actually electricity or hydrogen gas can be generated from

MFCs utilizing wastewater. If this kind of energy is collected efficiently, continuous energy supply can be expected for water recycling. B.E. Logan and his group[15,16] did lots of research on MFC applications to treatment of domestic sewage, industrial and other kind of wastewater, which described a realistic way of further development of MFC technology and drew much attention from scientists all over the world. As it is quite expensive to run a sewage treatment plant, it seems really attractive for governments if the plants can treat the wastewater using the energy produced by their own. Also with the development of industry and people's chasing for life quality, sewage discharge increases dramatically over time. In America, 1.125×10^{11} m^3 wastewater has to be treated every year and the cost of the treatment is more than 25 billion dollars, most of which is spent on plant operation. If we can further reduce the costs and improve the efficiency of MFCs, lower expenses on sewage plant operation could be expected in the future.

Besides, MFCs with different functions have been reported, including biological sensors that can determine the substrate content (such as sensors of lactic acid[17], BOD sensors[18], microbial fuel cells without media[19], non-traditional ceramic MFCs[20]). It is quite obvious that MFCs are becoming a hot research topic all over the world. As a project involving biology, chemistry, material, physics, and electrical engineering, MFCs can be further explored in many aspects to improve the efficiency and the power output. With advances in biochemistry and material fabrication techniques, we might be able to witness a faster development of MFC technology.

2.1.2 MFC basic principles

MFCs have various kinds of configurations. The most commonly used are two-chamber MFCs and air-cathode MFCs because they are easy to construct and operate. Figure 2.1 is

a typical schematic of a two-chamber MFC with a PEM membrane. The anode chamber should be kept anaerobically as diffusion of oxygen into it inhibits the electricity generation, while there is no specific requirement for cathode environment since it is pretty common to utilize oxygen as electron acceptors in cathode part, such as air-cathode MFCs[21]. A membrane is placed between anode and cathode chamber, to allow the diffusion of H^+ and prevent electron acceptors from coming into the anode part. Nafion is the most commonly adopted membrane in MFCs. As it is designed to transfer hydrogen ions, Nafion is recognized as cationic exchange membrane. Anode and cathode are connected to the external load with conductive wires.
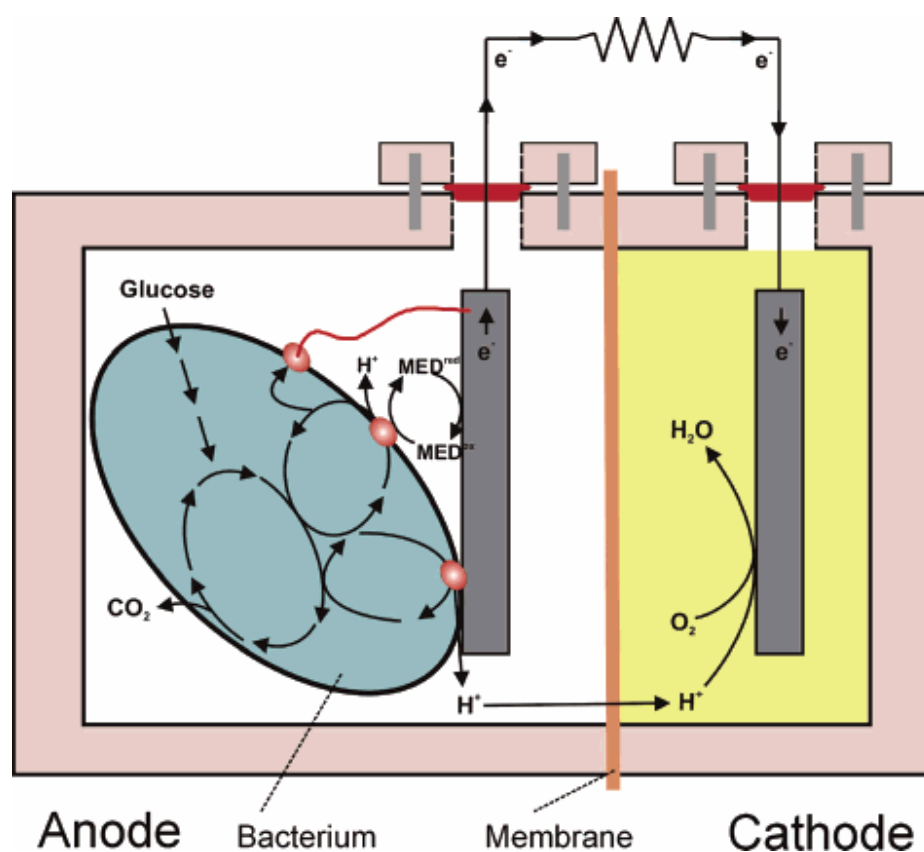
Figure 2.1: Schematic of a two-chamber MFC with a PEM membrane. Figure reprinted with permission from Ref. 16.

Taking glucose as example, the reactions occur in MFCs as follows:

Anode:

$$C_6H_{12}O_6 + 6H_2O \rightarrow 6CO_2 + 24H^+ + 24e^- \qquad (2\text{-}1)$$

Cathode:

$$6O_2 + 24H^+ + 24e^- \rightarrow 12H_2O \qquad (2\text{-}2)$$

Overall reaction:

$$C_6H_{12}O_6 + 6\ O_2 \rightarrow 6\ CO_2 + 6\ H_2O \qquad (2\text{-}3)$$
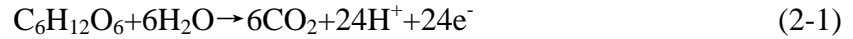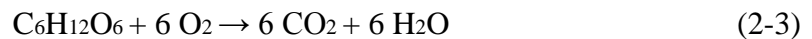
The mechanism of power generation of MFCs is explained as follows:

1) Microorganisms oxide organic matters (including glucose, protein, organic acid and so on) on the anode, producing CO_2, H^+ and electrons which are transferred to the anode surface.

2) The electrons produced go through anode, the external circuit and finally reach cathode. H^+ generated in the anode chamber is diffused to the cathode part through PEM and charge balance is achieved in the cathode chamber.

3) At cathode, electrons combine with H^+ and electron acceptors to form water. The whole process makes an electronic circuit and thus generates electricity.

In this process, the bacteria used to oxide the organisms are the key to power generation. This kind of bacteria capable of extracellular electron transfer are called exoelectrogens, most of which can grow anaerobically. The two most well-known exoelectrogen genera

are Shewanella and Geobacter[22,23]. There are many kinds of bacteria in Shewanella genera that are able to generate electricity, but the columbic efficiency is usually low compared with Geobactor (which can reach 99%). The mechanisms of extracellular electron transfer have been established based on the research on Shewanella and Geobacter and can be divided into two categories: direct and indirect electron transfer.

For direct interactions, proteins capable of electron transfer to the solid-phase electron acceptors are expressed by bacteria when the proteins and the acceptors (or anode matrix) are in direct contact. The mechanism requires the bacteria to have outer membrane redox cytochromes that enable electrons to be transferred to anode[24]. Besides, it has been proved that some bacteria can produce conductive nanowires to establish electrical connections with anodes (Fig. 2.2(b))[25,26,27].
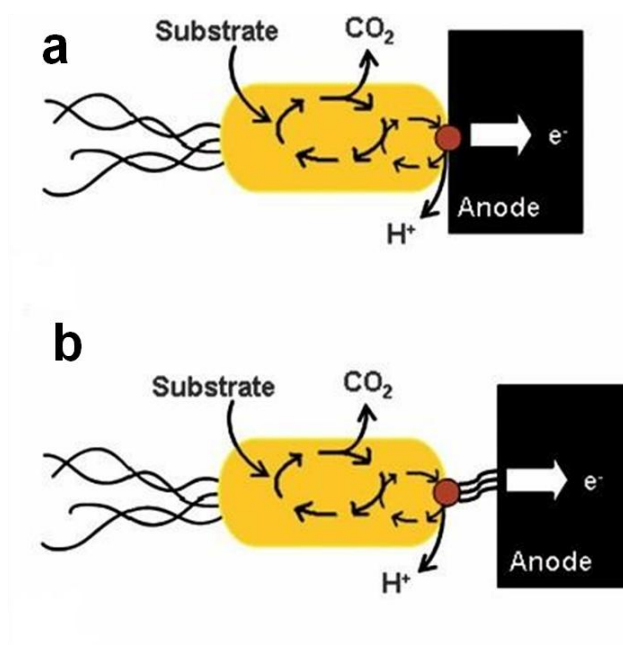
Figure 2.2: Schematic of direct electron transfer mechanism via (a) outer membrane cytochromes and (b) nanowires. Figure reprinted with permission from Ref. 25.
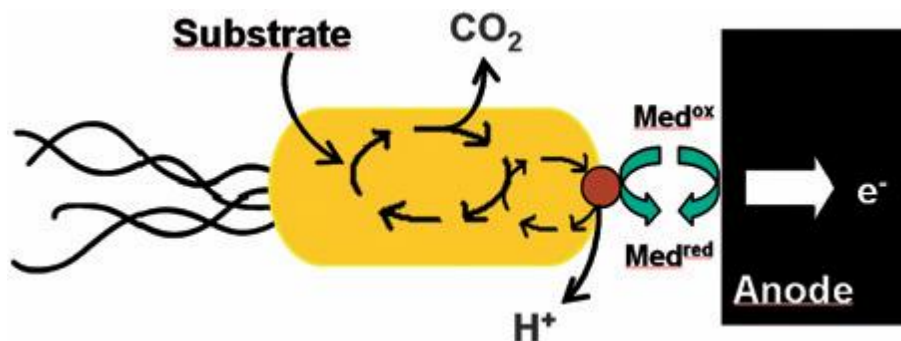
Figure 2.3: Schematic of indirect electron transfer mechanism via mediators. Figure reprinted with permission from Ref. 25.

For indirect electron transfer, the electron passage occurs by means of soluble redox minerals. These small molecules either are collected by chelate metals and delivered to an intracellular metal oxidoreductase or serve as electron shuttles by themselves (Fig. 2.3). These mediators can be exdogenous ones, which are natural or synthetic. The ideal MFC mediators must (1) be soluble and stable in water, (2) be able to go across the cell membrane, and (3) be reversible with electron accepting and donating.

H-type MFCs are often used in fundamental research such as testing the power output of new materials and the bacteria biofilm formation in some particular situations. The current produced by MFCs is calculated by the voltage over the external resistor, which can be collected by a potentiostat. We can then have the power output and the power density according to Equation 2-4,

$$P=U \times I=U^2/R$$

$$P_d=P/A \qquad (2\text{-}4)$$

where P and P_d represent power and power density, respectively, U is the voltage measured at the external resistor, R is the external resistor and A is the surface area of the electrode (usually projected surface area of anodes).

As the power output is affected by several factors, such as anode and cathode surface area, internal resistance of MFCs and ion exchange of membrane, electrodes and membrane with same surface area are used when comparing performances of different MFCs.

2.1.3   Anode materials in MFCs

In MFCs, what mainly determines the power output is the electron transfer onto anodes. Serving as the bacteria carrier, anode has a great influence on bacteria adhesion and the electrons transfer process from the bacteria to the anode. So it is of great significance to optimize the anode materials if we'd like to explore deeper into the mechanism of electron transfer and the effects of anode materials and surface conditions on bacterial growth. This would enable us to further enhance the performance of MFCs. There are several requirements for materials to function as anodes in MFCs such as high conductivity, high specific surface area, high porosity, good biocompatibility and low cost. Most of metal materials are great conductors, which are suitable for electron transfer. However, corrosion occurs when they are used as anodes for a long time. Besides, some metal materials are not good enough for bacteria adhesion, in which situation high electricity generation couldn't be expected, though they fulfill other requirements for MFC anodes. So it is quite important to examine the performance of different anode materials utilized in MFC systems.

(1) Carbonaceous anode

Carbon materials are the most widely used materials for anodes and cathodes in current MFC systems. Graphite plate[28], graphite granular[29], graphite felt[30], carbon paper[2], carbon cloth[31], carbon mesh[32], carbon brush[33], reticulated vitreous carbon (RVC)[34] and so on (Fig. 2.4) have been reported to serve as MFCs anodes[35].
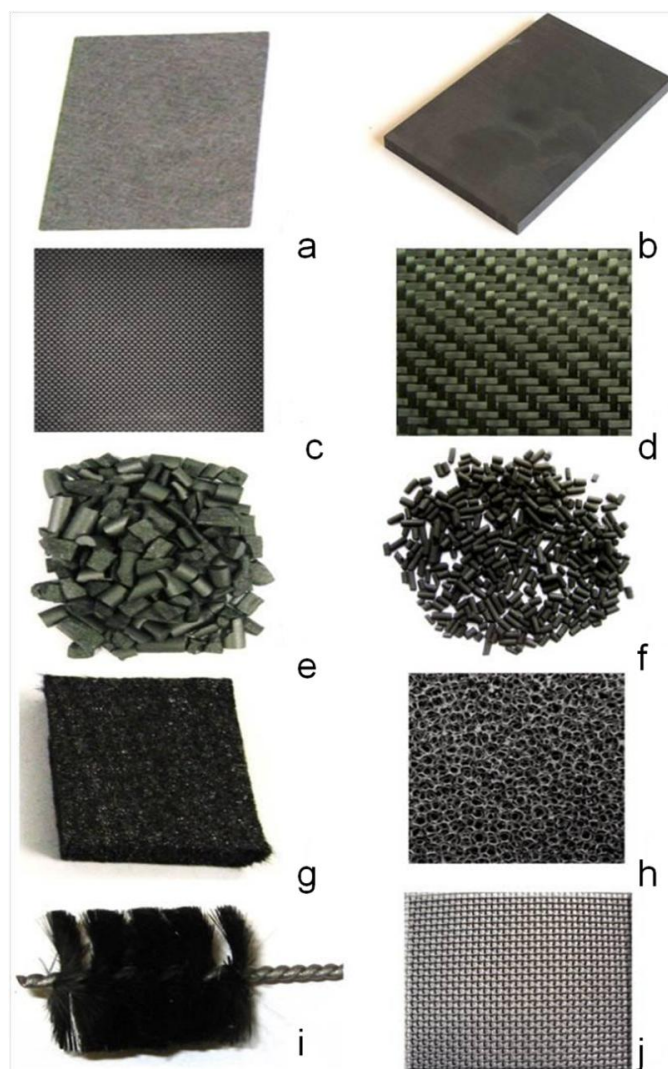
Figure 2.4: Electrode materials used for MFC: (A) carbon paper (B) graphite plate (C) carbon cloth (D) carbon mesh (E) granular graphite (F) granular activated carbon (G) carbon felt (H) RVC (I) carbon brush (J) stainless steel mesh. Figure reprinted with permission from Ref. 2.

Due to the relative high conductivity, good biocompatibility and cheap cost, carbonaceous electrodes remarkably satisfy most of the requirements of MFC electrodes. According to their configuration, the carbonaceous electrodes have been put into different categories: flat, packed and brush electrodes. Table 2.1 gives a brief description of some carbonaceous electrodes. Carbon paper and cloth, carbon mesh and graphite plates fall under the category of flat electrode configuration while carbon felt, RVC, granular graphite and graphite discs are usually packed electrodes. Carbon fiber brush and graphite fiber brush fall under the brush electrodes. The surface area can be dramatically increased if converting graphite anodes into fiber brush anodes, which compose distinct structures and are favorable for bacterial inoculation.

Table 2.1: A brief description of the MFC research with carbonaceous anodes

Anode	Fuel	Reactor type	Power Density	References
Carbon paper	Glucose	Single chamber	$262\pm10mW/m^2$	Ref. 19
Carbon cloth	Acetate	Double chamber	$112mW/m^2$	Ref. 29
RVC	Sucrose	Upflow	$170mW/m^2$	Ref. 32
Carbon brush	Acetate	Single chamber	$2.4W/m^2$	Ref. 31
Graphite felt	Glucose	Double chamber	$386\ W/m^3$	Ref. 28
Graphite plates	Lactate	Double chamber	$0.329mW/cm^2$	Ref. 26
Granular graphite	Glucose	Tubular MFC	$90\ W/m^3$	Ref. 27

Carbon fiber brushes are usually made by twining carbon fibers with several titanium wires. Due to their high surface area, MFCs using carbon brush anodes were found to generate a power density of 2.4 W/m^2, which is 4 times of MFCs with carbon cloth anodes. It's obvious that the bacterial adhesion on the anode surface plays a key role in electricity production. So it's essential to make some modifications to the anode materials so that bacteria can easily attach to the anode surface.

Chen et al. [36]reported a maximum current density of 30A/m^2 with 3D porous carbon fibers, which was produced by gas-assisted electrospinning, using wastewater as medium and microorganism source. This current density is almost 2 times larger than that achieved by using commercial carbon cloth foam anode. Further research on this anode found that bacteria grew on both the outer surface and the inner layers of this 3D porous anode, which formed bacteria biofilm and was thought to promote the current production. Mink and his group members utilized vertically aligned multiwall carbon nanotubes (MWCNTs) with a nickel silicide matrix to function as the microsized MFC anode, and a current density of 197mA/m^2 and a power density of 392mW/m^3 were achieved. Besides CNTs, graphene is also reported to have application in MFCs. Xie[37] reported one kind of MFC anode with graphene loaded onto 3D porous sponge and achieved good performance. They found that the mesoporous structures of the 3D porous sponge were ideal for bacterial adhesion and electron transfer between bacterial cells and electrodes, which helped enhance the anode performance of MFCs. Karra et al.[38] and Manickam et al.[39] reported microbial fuel cells using anodes made from activated carbon nanofibers (ACFs). Compared with activated carbon and carbon cloth, the efficiency and organic waste removal is greatly enhanced using ACF anodes. Though 3D porous anodes shown

above exhibit excellent MFC performances, the fabrication processes usually involve complicated physical and/or chemical operations, which largely increase the cost of electrode preparation and thus limit the potential of MFC scaling-up.

(2) Metal and metal oxide anode

Compared with carbonaceous materials, metal materials have better conductivity. However, fewer metal anodes have been applied to MFC systems due to the corrosion in MFC medium solution. The most commonly used metal materials are stainless steel and titanium.

Basically, it is difficult for bacteria to grow onto the surface of metal anode as it is quite smooth. Some research showed that the power output of MFCs with stainless steel anode was lower than that of MFCs with carbon anodes.[40] But when it comes to current density, metal anodes exhibit more potential than carbonaceous materials. Apart from stainless steel and titanium, nickel, gold and platinum electrodes were also utilized in MFC system[41,42,43], with power output similar to graphite electrodes.

Metal oxides recently attract lots of attention from researchers due to their pseudo-capacitance. Titanium dioxide[44], manganese dioxide[45] and ruthenium dioxide[46] have all been reported about their application in MFCs with a greatly enhanced power generation of $3580\pm130mW/m^2$. Actually, transition metal oxides like MnO_2 coated on conductive polymers such as poly-pyrrole (PPy) (or graphene, carbon nanotubes) are excellent materials to serve as anodes because of their quick and reversible redox behavior, huge surface area, and relatively high metallic conductivity[47]. Metal oxides are well recognized to have the capacitance typically 2-3 times larger than that of the carbon materials.[48]

More importantly, researchers[49] have demonstrated that metal oxides can interact well with bacteria and prompt electron transfer from the bacteria cells to the anode, which encourages us to make deeper exploration of these materials.

(3) Anode surface treatment and coating

As mentioned above, 3D porous structures help improve the efficiency of electron transfer and bacterial adhesion to anodes. Modified carbon or conductive polymer anodes have been introduced to MFC systems. Besides high surface area, modified anodes are able to decrease the energy status and thus reduce the potential loss and improve MFC efficiency. So research on modified anodes is one of the key steps to further enhance MFC performance.

1. Surface treatment

The surface treatment of MFC anodes mainly focus on acid etching, heat treatment, ammonia treatment at high temperatures, and electrochemical oxidation. Feng et al.[50] utilized inorganic acid and organic solvent for carbon electrode treatment, which removed the organism from the electrode surface. It has been reported that NH_3 gas was used to treat the carbonaceous anodes as well, which greatly enhanced the power density and reduced the setup time of MFCs owing to the improved conductivity and biocompatibility of anode materials. Saito et al.[51] further explored the effect of doped nitrogen on anode performance and discovered that the power density of MFCs could be as high as $938mW/m^2$ with a surface N/C atomic ratio 0.7, which was 24% higher than that with untreated carbon cloth. But if the nitrogen content was further increased, the

power density of MFCs decreased gradually. This shows only certain content of doped nitrogen can improve the anode properties.

Anode oxidation is also a commonly adopted method in electrode treatment. Zhou et al.[52] reported a power density of 792mW/m^2 from MFCs using HNO_3 treated anodes, which was 43% higher than untreated ones. 30mA/cm^2 constant current was applied to graphite plate anode by Tang et al.[53] before MFC operation and 39.5% power density increase was achieved. Further studies showed that microorganism adhesion and growth on the graphite anode surface was greatly enhanced after electrochemical oxidation. Liu et al.[54] utilized the similar method to treat carbon cloth and discovered that the specific surface area of carbon cloth anodes was increased after oxidation and amide groups were introduced to the anode surface, which improved the biocompatibility of the anode and bacterial adhesion.

2. Coating

Coating now is commonly used in electrode preparation. Carbon nanomaterials and conductive polymers are widely employed as matrixes in MFC anode modification to enhance the electron transfer and bacterial adhesion.

Since discovered, carbon nanotubes (CNTs) have become the most potential electrode material in different fuel cells and batteries, owing to their high specific surface area, high strength, good stability and conductivity. Peng et al.[55] utilized CNT modified glassy carbon anodes in MFC systems and studied the electron transfer process. The results turned out that the current density is 82 times larger than that of bare glassy carbon. 3D CNT-textile anode was also reported[56] to produce a power density of 1120mW/m^2, with

10-fold lower electron transfer resistance and 1.57 times higher current density than traditional carbon cloth anodes. Apart from CNTs, graphene has also received considerable attention. Zhang et al. used graphene to decorate the stainless steel anode and the power density of MFC based on this anode reached 2668mW/m^2. This was attributed to increase of electrode surface area.[57] Mesh like reduced graphene oxide (rGO) was also studied by Huang et al.[58] for the first time and they confirmed that rGO prompted the electron transfer to electrodes. The current density and the power density both increased about 4 times compared with carbon paper electrodes.

Coating of conductive polymers onto MFC anode surface has also received lots of attention from researchers, such as PANI and PPy[59,60], especially when introduced into MFC system with carbon nanomaterials. Nanoparticles are usually formed on the anode surface when coated with conductive polymers, increasing the surface area. CNT/PANI composite anode was first reported by Qiao et al[61]. They found the composite materials could enhance the charge transfer between E. coli and the anode. Composite with 20wt% CNTs had the highest electrochemical activity, producing a power density of 42mW/m^2 and a maximum voltage of 450mV. Zou et al.[62] studied the effect of CNT/PPy composite on the anode performance and a power density of 228mW/m^2 was achieved when 5mg/cm^2 CNT/PPy was loaded. As conductive polymers possess not only large surface area but also good biocompatibility, they serve well as bridges for charge transfer between bacteria and anodes and improve the performance of MFCs.

In summary, carbon materials, due to their low cost, good biocompatibility and stability, are still the first choice to make MFC anodes. It is estimated that the cost of anode materials is about 25% of the total cost of the large-sized MFCs, so how to fabricate

carbon anodes with low cost, high conductivity, high porosity and specific surface area in large scale is one of the key problems in MFC scaling up. CNTs and graphene are ideal materials in MFC electrode preparation except their high cost. However, 3D porous structures with different coatings are demonstrated to produce higher power densities compared with flat carbon materials, and are quite promising with further application in MFCs. Three-Dimensional printing technique, well-known for its precise printing of complicated and micro porous structures, is a new technology arising in recent years but its power has emerged in various fields. Utilization of 3D printing technique in MFC anode fabrication may enable us to fabricate 3D porous MFC anodes more easily.

2.2   Three-Dimensional Printing

3D printing is a manufacturing technique in which materials, like metal or plastic, are deposited layer by layer to fabricate three dimensional structures. This process differs from traditional printers which print in two dimensions (ink on paper). So far, 3D printing has mainly been used in engineering and fashion industry to create engineering models or jewelries. Besides, with the advance in printing materials and printer systems, 3D printers is able to produce objects that are comparable in precision with traditionally manufactured items. 3D printing is also believed to have the potential of mass production of customized goods on a large scale and thus named the key technology of the "Third Industrial Revolution".

2.2.1   Research Background

3D printing, also referred to as rapid prototyping (RP), additive manufacturing (AM), was first introduced by Charles Hull in the early 1980s.[63] In 1986, he developed the first

3D Systems and the .STL file format, which bridged computer aided design (CAD) software with transmit files for the printing of 3D objects.[64] The first commercial 3D printer, the SLA-250, was finally available to the public after further exploration. The first machine named "3D printer" was patented by MIT professors Michael Cima and Emanuel Sachs in 1993 to print different materials including plastic, metal, and ceramic parts.[65] Many other corporations, such as DTM Corporation, Z Corporation, Solidscape and Objet Geometries, have also developed commercial 3D printers. RepRap invented the first desktop 3D printer capable of printing out its own parts in 2008.[66]

Lots of applications of 3D printing technology have been found in automotive and aerospace industries for prototype printing of car and airplane parts. Other applications include printing structural models in architecture, gun prototyping and manufacturing in private and government defense. Beginning from early 2000s, 3D printing attracted the attention from medical industry, and dental implants and prosthetics were printed for the first time[67,68]. The applications of 3D printing also extended to food industry,[69] as well as in fashion[70],[71].

2.2.2   3D printing methods

In traditional printing industry, computer aided design programs are usually used to generate 3D models, such as AutoCAD, Solidworks, Catia. It is the same with 3D printing as the original designs are usually drafted in CAD programs, where they are then saved as .STL (Standard Tessellation Language) files for 3D printing. Plenty of 3D printing methods have been employed ranging from well-established methods, to recent developed techniques in research laboratories. In the following section, three most

popular systems will be introduced: stereolithography, selective laser sintering, fused deposition modeling, and laminate object manufacturing.

(1) Stereolithography

Stereolithography (SLA) was developed by Chuck Hull at 3D Systems[72] and was the first commercialized rapid prototyping method. Several different approaches to SLA have been developed such as direct laser writing (Fig. 2.5a) and mask-based laser writing (Fig. 2.5b).[73,74] In fact, all the approaches can be distinguished into bath configuration (Fig. 2.5a) or layer configuration (Fig. 2.5b) by the direction of the laser source. The direct laser writing usually has a movable base, a resin tank, a UV light source, and a computer interface while the mask-based writing is almost the same except having a "mask" called digital mirror device (DMD) which allows the model to be cured layer by layer.[75]
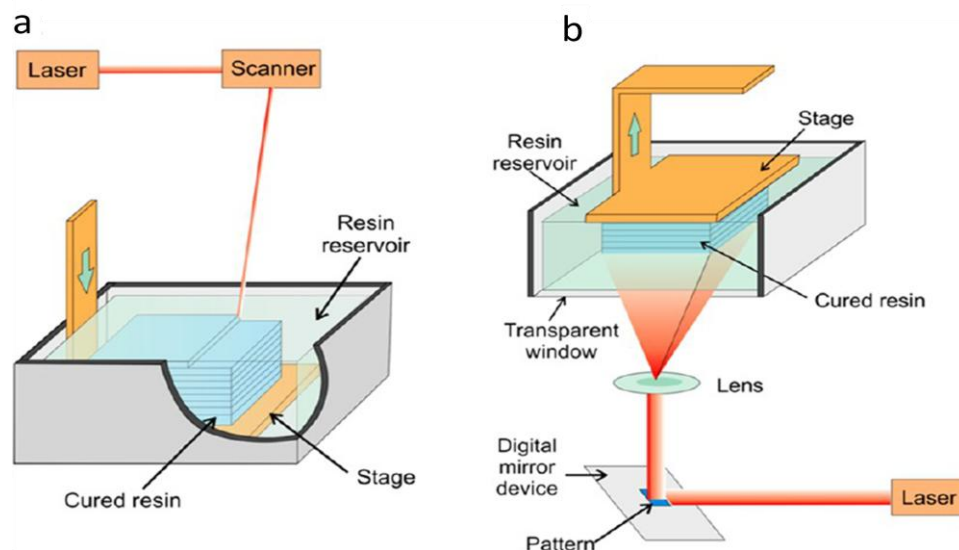
Figure 2.5: (a) Schematic of a bath configuration SLA printer with a direct writing process and (b) Schematic of a layer configuration SLA printer. Figure reprinted with permission from Ref. 75.

For the direct writing, the base was merged in a tank of liquid UV-sensitive resin that polymerizes upon UV illumination. The 2D cross section of the 3D model is traced by the UV beam and the resin is cured according to the design. Several factors decide the thickness of the cured resin involving exposure time, scan rate, and intensity of the light source. All of these factors are determined by the UV light energy to some extent. After the first layer of resin is completely cured, the base lowers into the resin again and on top of the first layer, the second layer is polymerized by the UV beam. Between each curing cycle, a blade, always keeping a level with the resin, is loaded to the resin surface. It is to ensure the liquid resin is uniformly loaded as a layer prior to UV light exposure, which is repeated layer by layer until the end of printing. Though bath configuration has several drawbacks such as limited object height owing to the size of the vat, extensive cleaning after printing and waste resin, it is the original printing system and leads to the creation of the layer configuration.[76]

The mask-based laser writing has the same components as the direct laser writing. However, the base is movable and held above the resin reservoir while the UV light source is placed beneath the tray, which is usually transparent. This configuration requires less resin compared with bath configuration. And as the base theoretically can be moved upward very high, there will be no problem printing parts with large heights. The printing process is almost the same as that of the bath configuration. First the movable base comes into contact with the resin followed by UV illumination. After the first layer cures, the base moves upward with liquid resin occupying the margin left from the cured layer. The process is repeated until the printing task is completed.[77]

The resolution of SLA printing largely depends on the UV light source. The most commonly used lasers are the HeCd laser and the xenon lamp. Resins are another limiting factor of SLA, as only one resin can be utilized in printing at a time. Thus functional design can be relatively difficult to complete. SLA 3D printers are usually quite expensive due to its high resolution (25μm/layer) but cheap desktop printers (~$2000) are becoming available in labs and personal offices with efficient (1.5cm/h) building speed.[78]

(2) Selective laser sintering

Selective laser sintering (SLS) was developed by Carl Deckard and Joseph Beaman from the University of Texas-Austin in the 1980s.[79] Similar with SLA, SLS uses lasers for printing. However, different printing materials are utilized in SLS including polymer powders or metal powders instead of liquid polymer resin (Fig. 2.6). So high power lasers, such as CO_2 and Nd:YAG,[80] are required to raise the temperature to the powders' melting point for material fusion according to the 3D design. One advantage of SLS printing is that no supporting materials are needed during printing process as the powders that are not sintered function as support material and are removable after printing.

Another advantage is the wide range of materials than can be used in SLS printing, including polycarbonate, PVC, nylon, ABS, metal and ceramic powders.[81,82] So polymer structures and metal structures could be directly printed out by this technique. However, since the laser and vibrating mirror system are quite different for polymer powder and metal power printing, SLS printers couldn't finish metal and polymer printing at the same time either. The resolution of SLS printing can be around 50 μm and is decided by several factors such laser power source and powder materials.
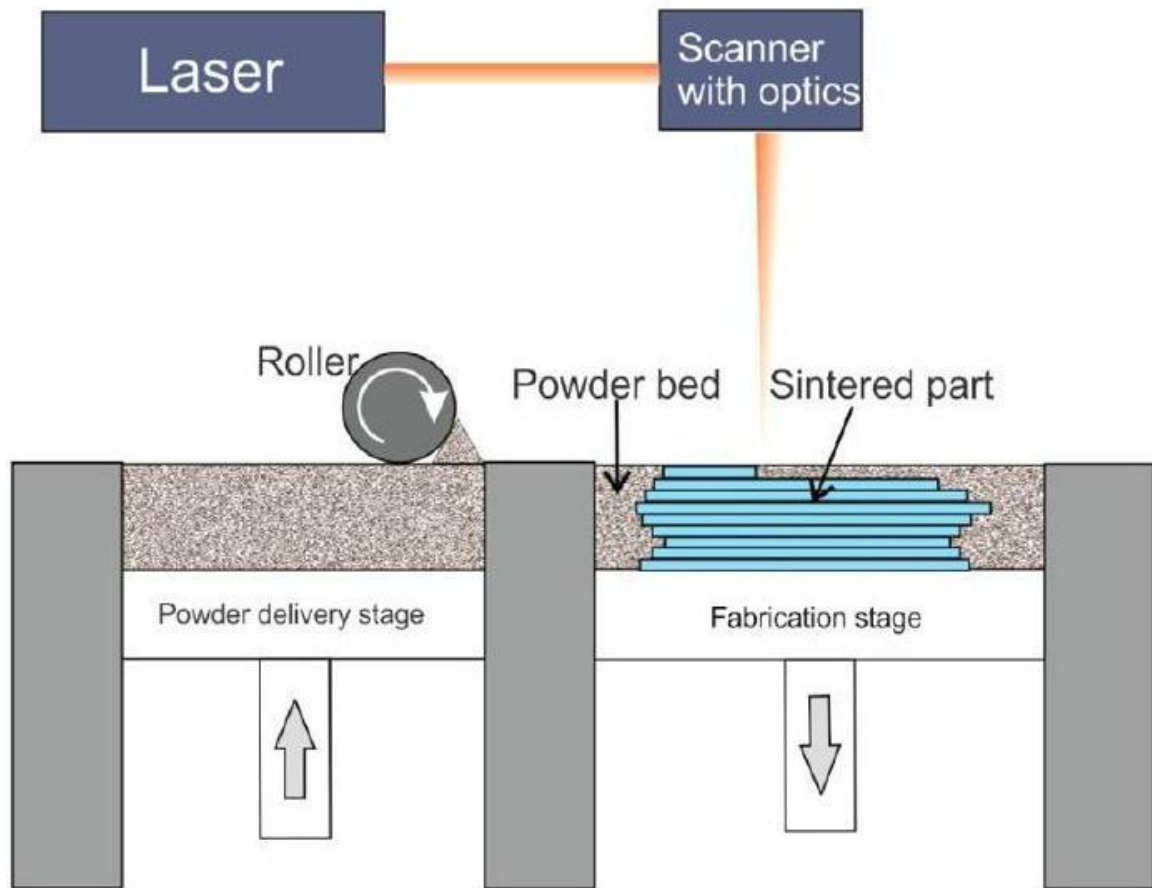
Figure 2.6: Schematic of SLS printer. The fabrication platform is lowered a predefined distance from its initial level followed by moving the powder material onto the stage with a roller. A laser then sinters the material according to the design. Figure reprinted with permission from Ref. 75.

(3) Fused deposition modeling

Fused deposition modeling (FDM) technique is a rapid prototyping technology developed by Stratasys Company in the late 1980s. FDM printing utilizes rolls of thermoplastic threads or metal threads for printing materials. The extrusion nozzle is heated to fuse the

thermoplastic materials followed by deposition of molten materials onto the platform (Shown in Fig. 2.7).[83,84]
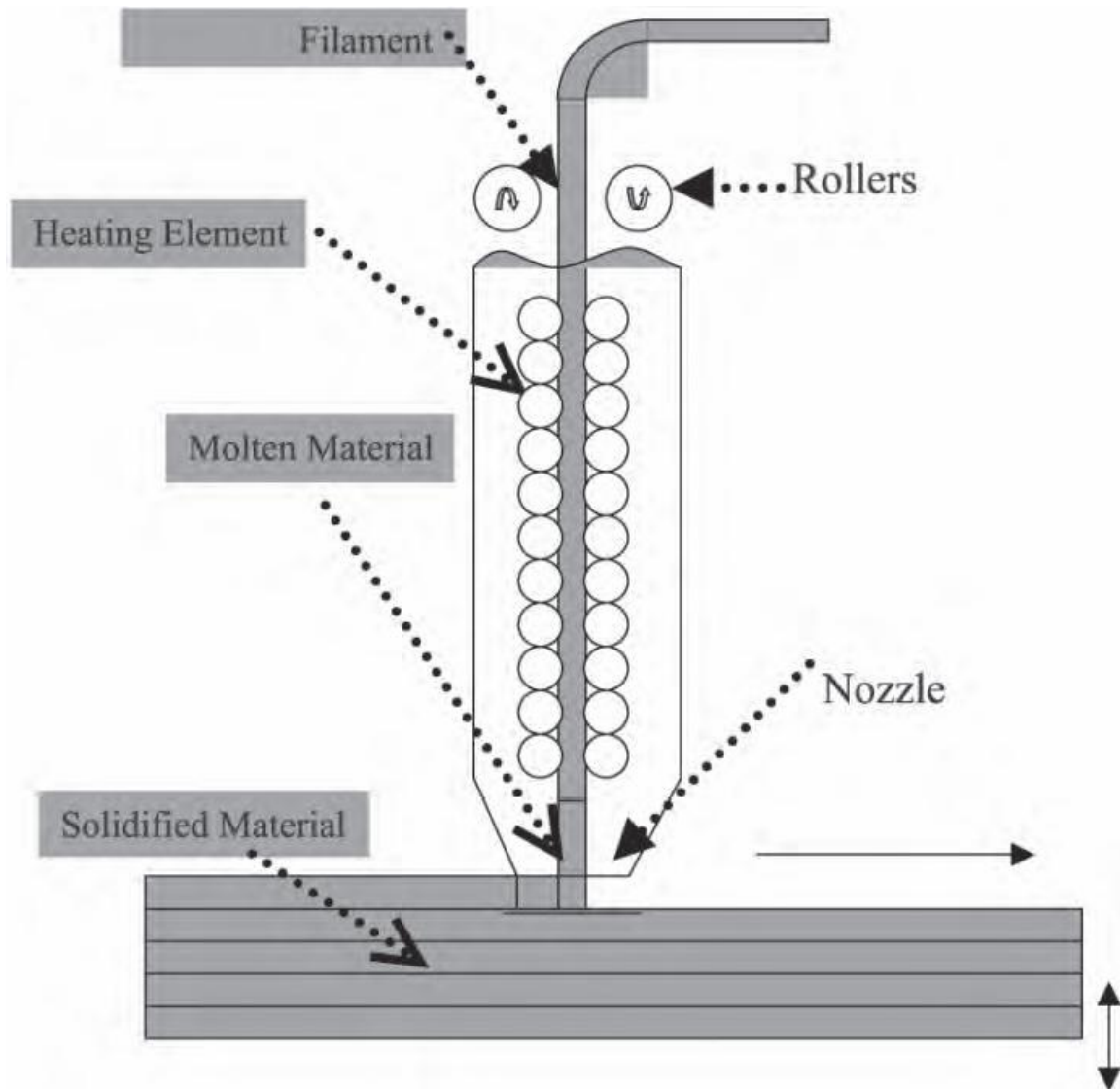
Figure 2.7: Schematic of an FDM 3D printer. Thermoplastic filament is heated to molten state before it is extruded from the nozzle and onto the platform layer by layer. Figure reprinted with permission from Ref. 84.

Compared with other 3D printing techniques, FDM is the only one that can use industrial thermoplastic materials for the layer-by-layer object printing, which means the wide

source of printing materials. Another obvious advantage of FDM is the larger printing size (914.4mm×696mm×914.4mm) with a resolution of 0.178mm compared with SLA and SLS. But the problem also coming with the relatively low resolution is the amount of defects. Lots of surface defects can be found after printing, which limits its application in precise printing area.

2.2.3   **3D printing application**

So far, scientists from different countries have been devoting most of their efforts to the improvement of 3D printing techniques, including resolution, printing materials and printing system design, and the application of 3D printing technology in industry. Due to its advantages in computer-assisted design, precise fabrication of micro scale structures and low cost, 3D printing has received wide recognition in product design and fabrication, and lots of product samples have been printed out by 3D printers.

Personal customization is the most obvious feature of 3D printed products. In 2013, the first metal gun M1911 pistol was fabricated by Solid Concepts using 3D printing technique. It took about 5 to 7 minutes to assemble more than 30 3D printed stainless steel and alloy parts[85]. In the aviation manufacturing industry, the cockpits, the airducts, the supports of the landing gear and the entire wings of the plane could all be produced by 3D printing. Besides, the production of these parts is usually quite small in traditional manufacturing due to its high cost, so 3D printing may fill in this gap as an attractive alternative.

Though mechanical parts could be easily fabricated by 3D printing, people are not just satisfied with this. People now are trying to use 3D printing to directly print PCB models,

which will improve the efficiency a lot. A new printing material called "carbomorph" has been developed by GKN aerospace and the University of Warwick, which indicates resistance changes when squeezed. The piezoresistive properties of this material further enable 3D printers to print electron components like functional buttons, switches and sensors.[86] Another 3D aerosol Jet printing technique has also been developed, capable of printing 3D circuits via 5-axis motion and multilayer devices with printed electronic materials.[87] This technique is quite different from the common 3D printing methods using liquid or solid printing materials as liquid electronic material is jet grouted into gas state, followed by deposition of this gas electronic material on the platform layer by layer with a resolution as low as 10 μm.

Table 2.2 Estimated 3DP market potential in various fields (in billion US $).

Market		Consumer products	Aerospace industry	Automotive industry	Medical components	Tooling	Source
Market potential	Low	100	58	5	38	30	Ref. 81, 82
	High	300	116	10	76	50	

Personal customization of 3D printing technique also has great applications in medical industry. Human skin, bones and other organs and tissues have been printed out by bio 3D printers. [88] A small portion of skulls and artificial limbs printed by 3D printers have been utilized for medical replacement of patients' corresponding parts, since the customized printed medical devices can better satisfy the needs of patients.

Table 2.2 below lists the potential market of 3D printing in different fields.[89,90] Though there are still lots of problems with 3D printing, the market potential of 3D printing by 2025 is quite promising, estimated to reach 230-550 billion US dollars. [91]As 3D printing is becoming more and more popular both in research and in industry, more applications in other fields will be found for it.

This thesis is about to find its first application in microbiology and environmental science.

Chapter 3

3 Fabrication of 3D Printed Porous Anode with Copper Coating and its Application in MFCs

It has been stated in last chapter that 3D porous anodes are one of the key components that can efficiently improve the bacteria adhesion and MFC performance. In this chapter, a brief introduction to copper electroless plating is given, followed by the detailed fabrication process of 3D printed porous anodes with copper coating and MFC construction. In addition, various testing techniques used in collecting voltage data from MFCs, obtaining power densities, as well as charactering the biofilm formation on anodes are discussed. In order to detect copper corrosion, energy-dispersive X-ray (EDX) and inductively coupled plasma mass spectrometry (ICP-MS) are also introduced.

3.1 Introduction

Electroless plating, a commonly used method for fabricating thin films of metals and alloys, is a highly selective way to allow isolated and embedded patterns on different insulating materials, such as polymer, plastic and glass. It is a very mature technology with a quite long history, dating back to the early 19th century. Nickel electroless plating was first reported by Wurtz[92] who used sodium hypophosphite to serve as a reducing agent for nickel plating in 1844. The term "electroless plating" emerged much later in 1947 by Brenner and Riddel[93,94]. In the late 20th century, electroless plating began to find its application in microelectronics revolution, providing various solutions to lots of micro and nano technology applications such as 1 micro scale integrated circuits, supporting the "Moore's law". For electroless plating, the equipment and systems are much simpler

compared with chemical vapor deposition (CVD) and physical vapor deposition (PVD). Electroless deposition usually consists of relative low temperature controlled bath, sample holder, solution preparation, sequencing, monitoring and control.

Copper, silver and gold are the commonly deposited by electroless plating using aqueous solutions, due to their excellent conductivity. Some metals or alloys with lower conductivity, like nickel or cobalt and their alloys, are also coated as diffusion barriers in microelectronics. Electroless plating has been widely utilized for packaging and printed electronics[95], and also been studied for Integrated Circuits (IC) and 3D integration. We choose copper for metal coating on 3D printed porous structures, since it is the metal selected for most electroless plating micro and nano scale applications. Recent advances in copper electroless deposition technology can be found in many papers and in books by Shacham-Diamand[96]and Murarka[97]. Alloys, due to its higher specific resistivity than pure metals, are suitable for low current density or protective coating applications.

3.2 Experiment

3.2.1 **3D printed copper anode preparation**

As stated in previous chapters, porous anodes of MFCs play a significant role in improving MFC performance and a too large or too small pore size may not be ideal for bacteria growth. As there were few papers reporting porous anodes structures with pore sizes between 10 μm and 550 μm, in this thesis, 3D porous anode substrates with a pore size of 500 μm were printed. The porous anodes were 2.75 cm in diameter and 0.5 cm in thickness, and the 3D printer (Fig. 3.1) with UV curable resin was purchased from Asiga.

Figure 3.1: Asiga Pico SLA 3D printer and the platform where the 3D structures could be printed.
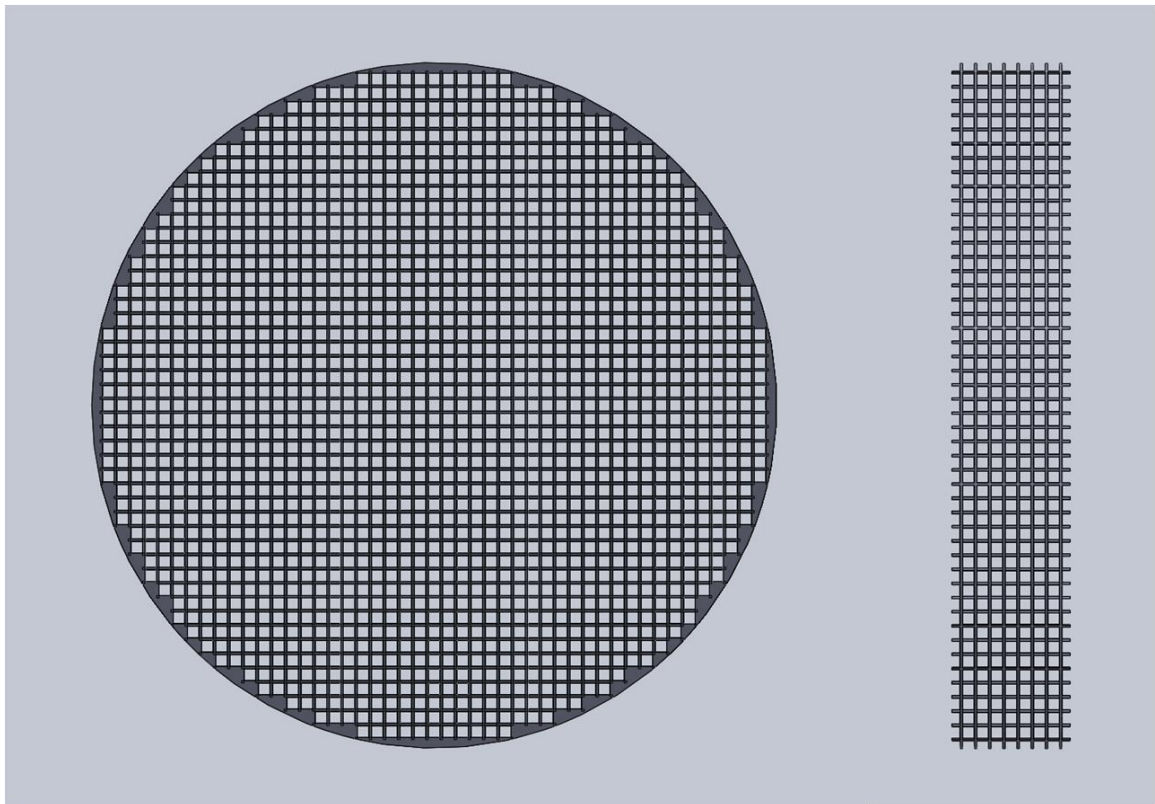
Figure 3.2: Lattice structures designed by Solidworks software.

Lattice structures were adopted due to their periodicity which helped reduce the cost of structure design and fabrication, and designed by Solidworks software (Fig. 3.2). The designed structures were saved as .STL files before transfer to 3D printing program. These structures were printed with a layer thickness of 25 μm with burn-in exposure and normal exposure time both 1s. The platform of the 3D printer was cleaned with ethanol and washed 3 times by DI water. It was blow-dried before it was placed to the 3D printer.

After the anode structures were printed out (shown in Fig. 3.3a), they were treated by sonification in ethanol for 10 min. The substrates were washed 3 times by DI water before they were immersed into a 2.5g/L lead acetate acetone solution for 20 min. The $Pd(Ac)_2$ thus infiltrated the surface of the 3D printed matrixes with the diffusion of acetone. The samples were again rinsed with DI water and the $Pd(Ac)_2$ loaded samples were then immersed into the copper plating bath, which contains a 1:1 mixture of freshly prepared solution A and B. Solution A consisted of 14g/L $CuSO_4 \bullet 5H_2O$, 20g/L EDTA•2Na, 11g/L sodium hydroxide, 20 mg/L 2,2'-dipyridyl, 10 mg/L potassium ferrocyanide and 16 g/L potassium sodium tartrate. Solution B is 16.5 ml/L methanal in DI water. After copper electroless plating, the samples were rinsed by DI water again to make sure all unbonded copper ions were washed away. The anode samples before and after copper electroless coating are shown as Fig. 3.3 (a), (b).

For comparison purpose, anodes made from copper mesh (50×50, opening size: 30 μm, McMaster-Carr) and carbon cloth (Fuel Cells Etc) were also fabricated with a 2.75 cm diameter and a project area of 6cm^2. All kinds of anode structures were autoclaved at a temperature of 121℃ before application in MFCs.
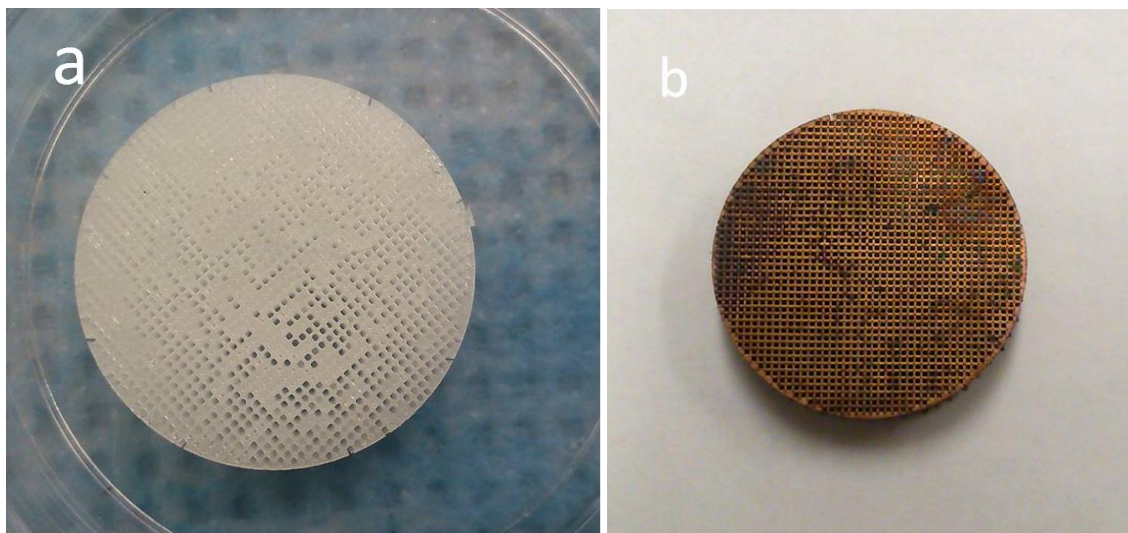
Figure 3.3: 3D printed porous anode substrates (a) before and (b) after copper electroless plating.

3.2.2   **Shewanella oneidensis MR-1 cultivation**

Shewanella oneidensis MR-1 was cultured aerobically in a water bath shaker (New Brunswick Scientific Gyrotory, Figure 3.4(a)) for 3 days at a constant temperature of 30℃. Agitation was maintained at 150 rpm, to make sure of intensive mixture of bacteria and medium. Tryptic Soy Broth (TSB, BD) is used as bacteria medium. The bacteria were collected by centrifugation (5000 rpm, 6 min, Fig. 3.4 (b)) and washed three times in PBS buffer (Dulbecco's, Sigma) before adjusting to the desired cell concentration (OD600 0.4). The washed cells were inoculated in another growth medium same as that used by Bretschger et al. with 18mM lactate.[98] The chemically defined medium used, contains the following: 18 mM sodium lactate, 50 mM PIPES buffer, 28 mM ammonium chloride, 4.35 mM NaH_2PO_4, 7.5 mM sodium hydroxide, 1.3 mM potassium chloride,

100 mM sodium chloride. 10 ml of $10\times$ vitamin solution (ATCC MD-VS), and 10 ml of $10\times$ trace mineral solution (ATCC MD-TMS) are added to the medium later by sterile filtration (0.2 μm, VWR). The vitamin solution (per liter of deionized water) contains 2.0 mg folic acid, 10.0 mg pyridoxine hydrochloride, 5.0 mg riboflavin, 2.0 mg biotin, 5.0 mg thiamine, 5.0 mg nicotinic acid, 5.0 mg calcium Pantothenate, 0.1 mg vitamin B12, 5.0 mg p-Aminobenzoic acid, 5.0 mg thioctic acid, 900.0 mg monopotassium phosphate, which are based on Wolfe's vitamin solution. The trace mineral solution (per liter of deionized water, also based on Wolfe's mineral solution) contains 0.5 g EDTA, 3.0 g $MgSO_4 \cdot 7H_2O$, 0.5 g $MnSO_4 \cdot H_2O$, 1.0 g NaCl, 0.1 g $FeSO4 \cdot 7H2O$, 0.1 g $Co(NO_3)_2 \cdot 6H_2O$, 0.1 g $CaCl_2$ (anhydrous), 0.1 g $ZnSO_4 \cdot 7H_2O$, 0.010 g $CuSO_4 \cdot 5H_2O$, 0.010 g $AlK(SO_4)_2$ (anhydrous), 0.010 g H_3BO_3, 0.010 g $Na_2MoO_4 \cdot 2H_2O$, 0.001 g Na_2SeO_3 (anhydrous), 0.010 g $Na_2WO_4 \cdot 2H_2O$, 0.020 g $NiCl_2 \cdot 6H_2O$.
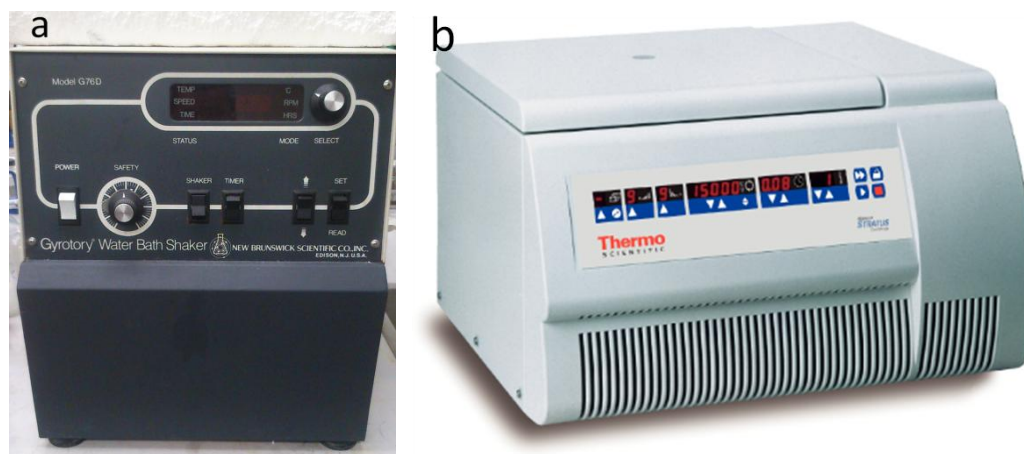
Figure 3.4: (a) Water bath shaker employed for cultivation of MR-1, (b) Centrifuge (Biofuge™ Stratos™ Centrifuge Series, Thermo Scientific) for bacteria cell centrifugation.

The MR-1 cultivation was operated in batch mode. The growth conditions in batch culture changed continuously as no additional TSB medium was added to the cultivation medium. The cell densities were measured at 600 nm with a UV/Vis spectrophotometer. It took about 3 days for the cell densities to reach 0.4 at 600nm.

3.2.3 MFC construction and setup

In this thesis, air-cathode MFCs are employed for measurement and comparison between each other. Chambers of the same size (4 cm long, 3 cm in diameter, 28 ml volume, Phychemi (Hong Kong) Company Limited) are used for MFCs with various anodes (Figure 3.5(a)). The air-cathode was gas diffusion layer (7 cm^2) made from woven carbon cloth and coated with 0.5 mg/cm^2 of Pt (Fuel Cells Etc). The spacing between the anode and the air-cathode is 2cm. All MFCs were sealed by epoxy and dried before use (Figure 3.5(b)).
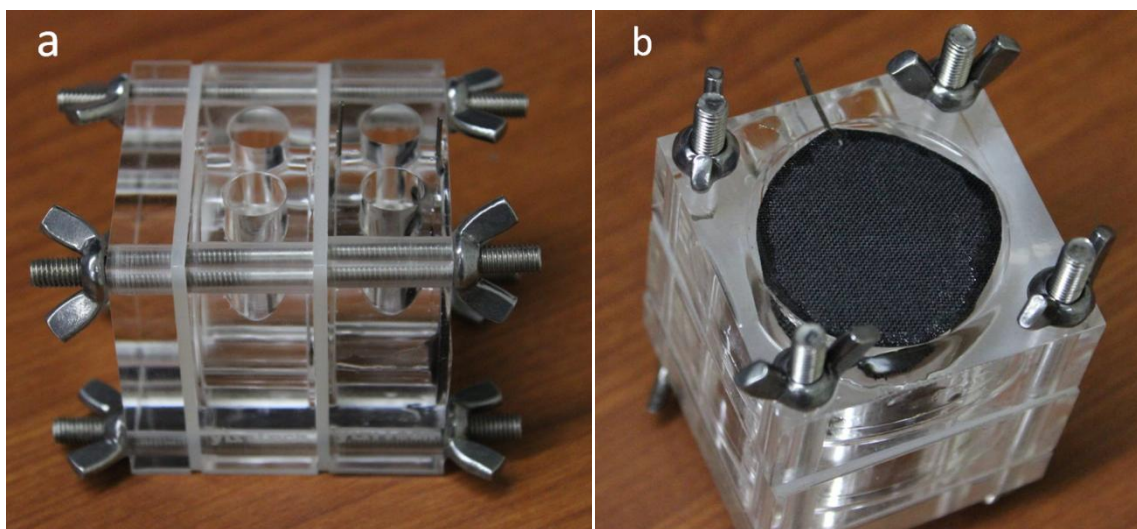
Figure 3.5: (a) Air-cathode chamber with two inlets and outlets, (b) carbon cloth cathode with 0.5 mg/cm^2 of Pt on Vulcan, sealed by epoxy.

Three air-cathode MFCs were constructed with the 3D printed porous anode, copper mesh anode and carbon cloth anode fabricated above. All components were autoclaved before bacteria inoculation. The bacteria cultivation medium prepared above was used for MR-1 culture inoculation. The medium used for MR-1 test was the same as the growth medium used above. After adding lactate, the medium was adjusted to pH 7 by 2M HCl.

MFCs were inoculated with 50% inoculum of S. oneidensis MR-1 and medium. All MFCs were connected to a 1000Ω external resistor. The solution in MFCs was replaced every 2.5 days until MFCs produce relatively stable voltage and then only fresh medium was added over the following fed batch cycles. Medium replacement was conducted in a laminar flow hood (Forma Class II, Biological Safety Cabinet, Thermo Scientific). All the three MFCs were operated at room temperatures ($20\pm2\,℃$). The MFCs were ready for testing and considered enriched once they achieved similar maximum voltage for four consecutive batch cycles (about 15 days for air-cathode MFCs).

3.2.4   **Characterization**

(4) Voltage

The cell voltages (mV) across a 1000 Ω external resistor in the circuit was monitored every 5 min using a high –resolution DAQ device (USB 6251 BNC, National Instrument) and the LabVIEW software package (National Instruments). The voltage measurement system (Figure 3.6(a)) was self-designed and worked well to complete the monitor task. The DAQ device was connected to a computer and controlled by LabVIEW program (Figure 3.6(b), (c)).
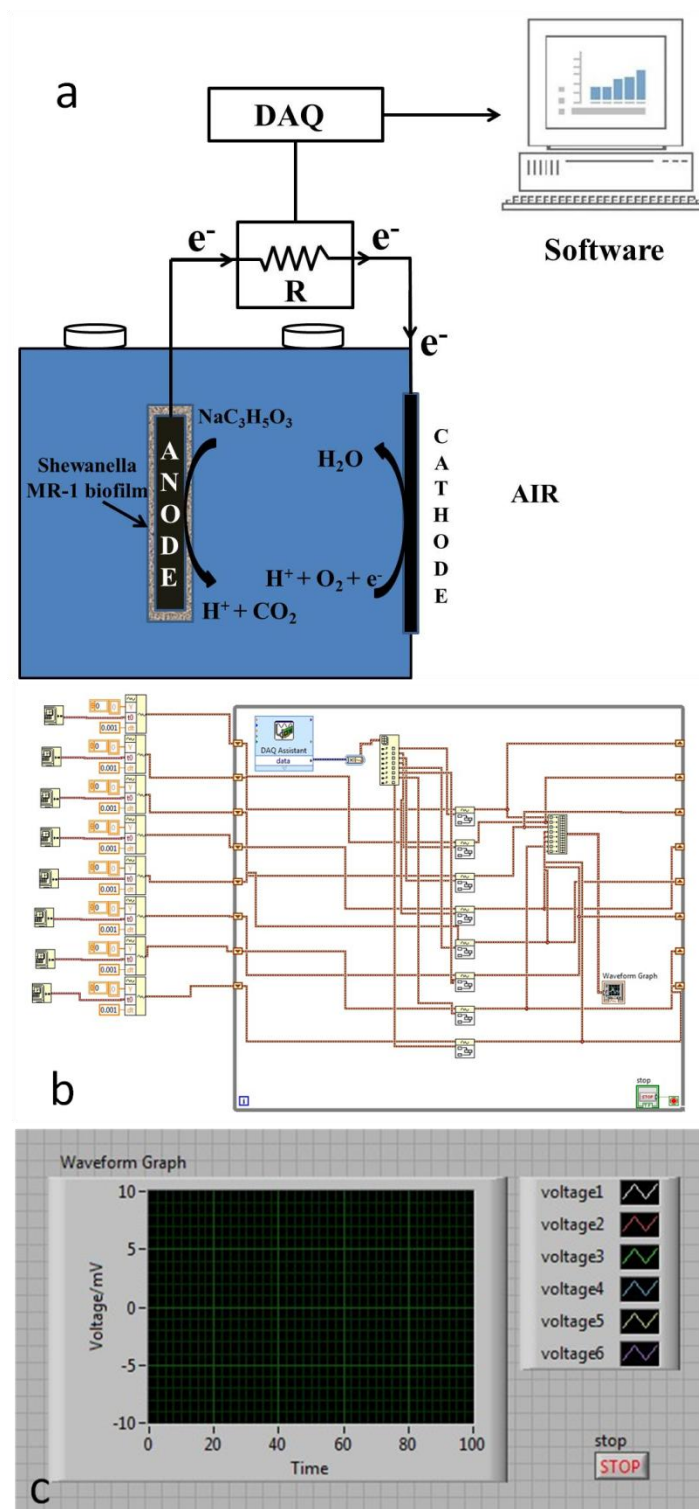
Figure 3.6: (a) Schematic of self-designed voltage measurement system, (b) block diagram and (c) front panel of the LabVIEW program designed for voltage measurement system.

(5) Linear sweep voltammetry (LSV)

Linear sweep voltammetry (LSV) was conducted with a potentiostat (CHI 1200a, CH Instruments Inc.) by setting MFCs at their open circuit potentials (OCP) for 40 minutes, and scanning the voltage from OCP to -10 mV at a rate of 0.1mV/s, with the anode serving as working electrode and cathode serving as the counter and reference electrode. Power densities were calculated using Equation 2-4:

$$P=U \times I=U^2/R$$

$$P_d=P/A \qquad\qquad (2-4)$$

where A is the anode projected surface area (6 cm^2). The peak power densities for MFCs with different anodes always fall at the middle of the scanning range.

(6) Copper corrosion

In this thesis, copper ion concentration in the chamber was tested by inductively coupled plasma mass spectrometry (7700x ICP-MS, Agilent Technologies), to determine whether copper corrosion happened. ICP-MS is one kind of element spectrometry which is capable of detecting both metals and several inorganic elements at concentrations as low as 10^{-15}. Such high resolution is achieved mainly because of ionization of the sample with inductively coupled plasma, followed by using a mass spectrometer to separate and quantify those ions.

Compared to other element detecting techniques based on atomic absorption, ICP-MS has several advantages, such as greater precision, faster speed, and better sensitivity.

However, ICP-MS also presents some problems compared with other types of mass spectrometry and it sometimes introduces a lot of interfering elements to samples: component gasses of air through the cone pore, argon from the plasma, and contamination from glassware.

Energy-dispersive X-ray (EDX) was employed to further evaluate the copper coating on 3D printed anodes before and after MFC operation. EDX is a technique commonly used by researchers for the elemental analysis of a sample. The results reflect the interaction between X-ray excitation and samples. And its characterization capabilities are largely based on the fact that the atomic structure of each element is quite unique, which stands for certain peaks on X-ray emission spectrum.[99] A beam of high-energy particles such as electrons is guided to hit the sample to excite the emission of certain typical X-rays from some area on the sample surface. The emission of the X-rays is mainly caused by the difference of electron energy states between the inner shells and the outer shells of an atom. The incident high-energy beam used may excite electrons in a lower energy shell and eject them to outer shells at the same time create a hole where the electron was. And then electrons from a higher-energy shell may find ways to fill the hole, releasing energy difference in the form of an X-ray. As the atomic structure of each element is quite unique, the number and energy level of the X-rays emitted from a sample can be very different and thus the elemental composition of the sample can be clearly known.

(7) SEM biofilm characterization

After various measurement and tests were conducted to MFCs, the anode structures were taken out of MFCs chambers and examined by scanning electron microscopy (SEM).

Special preparation processes and treatments are usually required for biological specimens before SEM in order to preserve the certain morphology of samples in some certain environments and enhance the imaging quality.

SEM has been used to characterize bacterial cells and their ultrafine structures such as bacterial nanowires for many years.[100,101] A beam of high-energy electrons are employed to scan the specimen in SEM and images the surface morphology in a raster scan pattern. The high-energy electrons (on the order of keV) interact with the sample surface, producing various signals that contain information about the surface features, specimen composition, and other properties. Samples are usually required to be electrically conductive and grounded before they are sent into SEM chamber. So non-conductive specimens like bacteria biofilms must be deposited with conductive materials, such as platinum, carbon and gold, onto the surface to prevent the accumulation of electrostatic charge. Since high vacuum (on the order of 10^{-5} to 10^{-7} Torr) is required for the working chamber of SEM, samples are usually required to be one hundred percent dry. Therefore, chemical fixation and dehydration treatment procedures are often needed to preserve biological samples and stabilize their structures.

After three different kinds of anodes were taken out of MFCs, SEM was used for assessing whether bacterial bioflim was formed on the surface of top layers or inner layers of porous copper anodes. Anodes (with potential biofilm) were first washed three times in pH 7 phosphate buffer solution (PBS) to remove organism remained and then chemically fixed with 3% glutaraldehyde. The solution was kept in a refrigerator overnight at 4℃. Fixation is usually employed to preserve biological samples in their

natural states for scanning electron microscopy and other characterization. After chemical fixation, the bacterial biofilm on anodes was rinsed softly in pH 7 phosphate buffer solution (PBS), and then diluted PBS (1:1 with distilled water) and DI water. A graduated series of ethanol solution with increasing concentrations (20%, 40%, 60%, 80% and 100%) were utilized to dehydrate the anodes. After rinsing in 100% ethanol for three times, the specimen were dried in a vacuum chamber. Samples were then deposited with a thin layer of gold in a sputtering coating chamber and examined on a Hitachi S-4500 field emission SEM with a Quartz PCI XOne SSD X-ray analyzer.

3.3   Results and Discussion

MFCs with different anodes were operated more than 40 days with medium replaced every 28 hours, but the performance of each MFC was quite different at first several cycles. MFCs that had 3D printed copper anode and copper mesh anode immediately produced high voltages when connected to the external resistors (1000Ω), which was also reported by Logan's group[102]. The maximum voltage obtained during the first cycle was 224.5mV for the 3D printed anode and 179.1mV from the MFC with a copper mesh anode, and then the voltages dramatically dropped to 95.2mV and 45.2 mV, respectively (Fig. 3.7(a) (b)). After about ten cycles, the maximum voltages of MFC with 3D printed anode stabilized at 65.7±3mV while only 7.6±0.5mV was achieved for copper mesh anode over successive cycles. MFCs with carbon cloth anode initially generated very low voltages (Fig. 3.7(c), similar to MFC with carbon cloth anode but inoculated only twice as shown in Fig. 3.7(d)). However, the maximum voltage increased to over 191.5mV after 15 cycles and stayed at 190±5mV afterward.

Clearly, voltages produced by MFCs with carbon cloth anode are much larger than that of MFCs with copper anodes. However, 3D printed porous copper anodes demonstrated better performances compared to copper mesh anode. The maximum voltage 65.7 ± 3mV produced was about 9 times larger than that produced by copper mesh anode and 20 times larger than what has been reported by Logan.
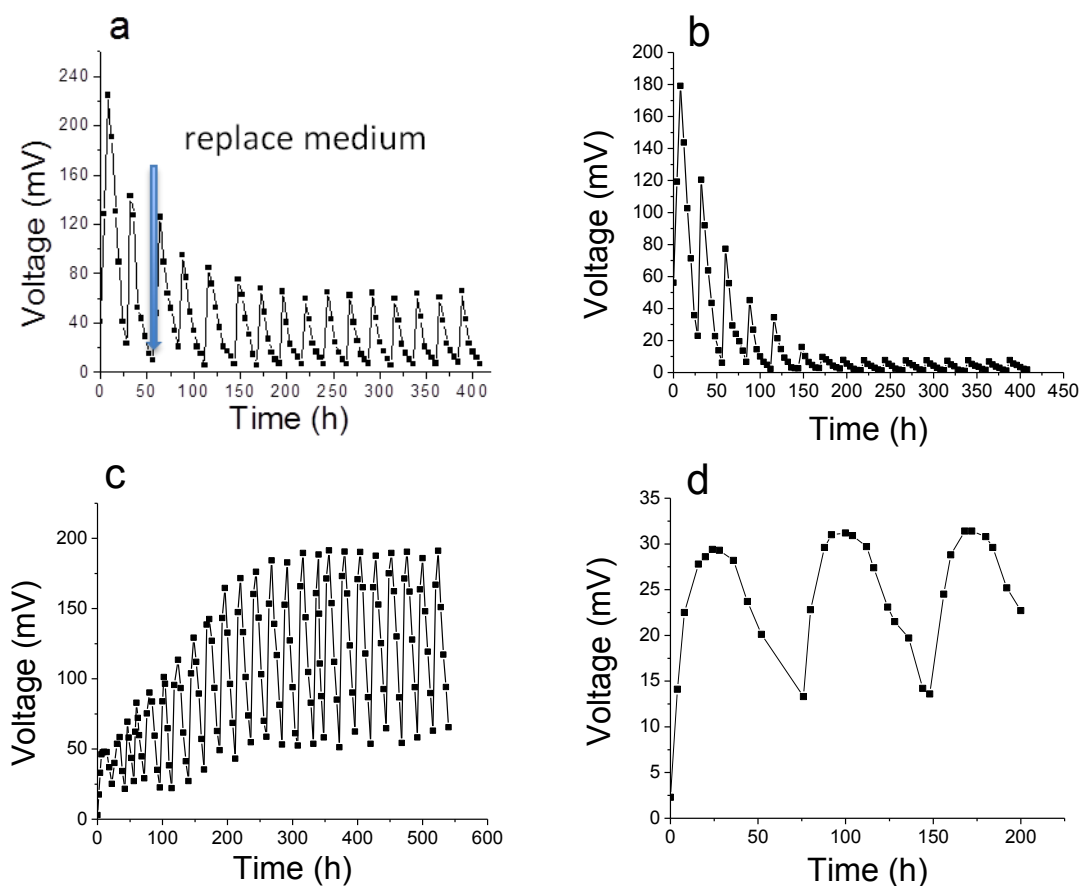
Figure 3.7: Voltage production of MFCs with (a) 3D printed copper, (b) copper mesh, (c) (d) carbon cloth anodes with 1000Ω external resistors. The first three pictures shows voltage produced by MFCs considered enriched as they reached stable maximum voltage for several cycles and (d) presents the MFC inoculated with 50% MR-1 culture and medium only twice.

Polarization curves plotting voltage as a function of current are commonly utilized to analyze and characterize MFC performance.[103] In this study, they were measured when the maximum voltages generated by all MFCs were repeatable over successive cycles, in order to evaluate the influence of copper element and porous structures on anodic electrochemical behavior of MR-1 fed by lactate. Dual-electrode mode was adopted in polarization curve measurement with the three different types of anode materials serving as the working electrodes, while the reference and counter electrodes were same for the entire three MFCs, woven carbon cloth cathode coated with 0.5 mg/cm^2 Pt/C. The polarization curves obtained were listed as follows (Fig. 3.8 (a) (b) (c)). The open circuit potentials for three MFCs with different anodes are 0.435V, 0.460V and 0.673V, respectively.

How to calculate the power densities based on polarization curves is presented above. The maximum power density generated by MFC with 3D printed copper anode was 6.45±0.5 mWm^{-2}, compared to 0.53±0.04 mWm^{-2} for copper mesh anode and 69.0±2 mWm^{-2} for carbon cloth anode (as shown in Fig. 3.8 (d) (e) (f)). Logan's group reported a power output of 2±0.3 mWm^{-2} based on a copper mesh anode and effluent from other MFCs. It was obvious that 3D printed anodes could help enhance the power generation of MR-1 MFCs as the power density for 3D printed anode was more than 3 times larger than the figure above, let alone the low coulombic efficiency of MR-1 (16%) ever reported[104]. Same conclusion could be drawn in this study as MFC with 3D printed anode produced about 12 times higher power density than that with copper mesh anode, though power output from both of them was at least one order lower compared to MFC with carbon cloth anode.
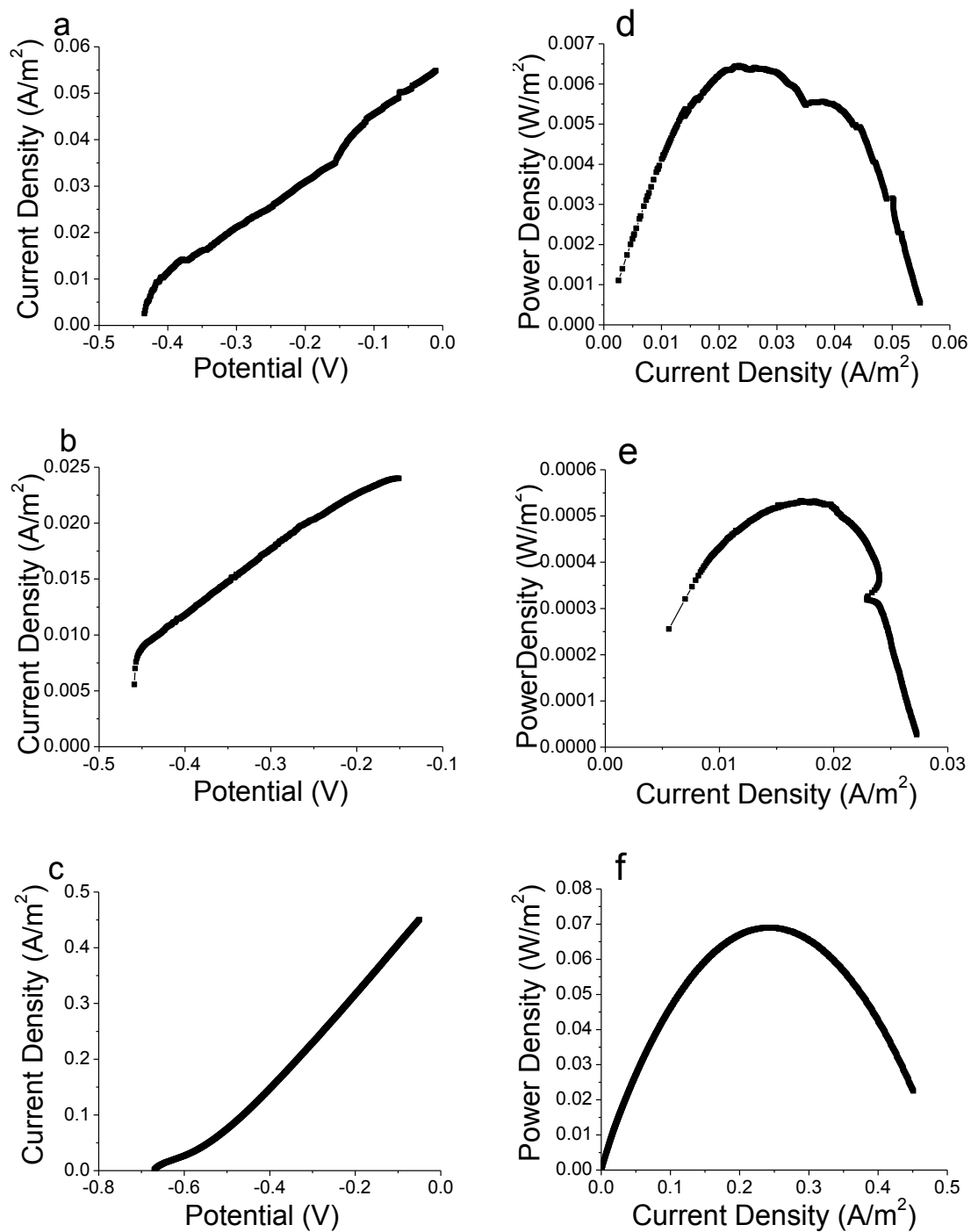
Figure 3.8: The polarization curves measured for MFCs with (a) 3D printed porous copper anode, (b) copper mesh anode, and (c) carbon cloth anode. The corresponding power density curves of each MFC as a function of current density are plotted as (d), (e) and (f), respectively. Both the power density and current density are based on the same projected surface area of anodes (6cm^2).

The main reason for higher power density with 3D printed anode than copper mesh was partially because of the higher surface area than copper mesh (Fig. 3.9). The 500 μm pores were well printed out at first, with layers of copper coated afterward. From Fig. 3.9 (a), we could clearly find that the pore size of the 3D printing structures was precisely controlled even after copper electroless plating. Apart from the microporous structures, the high-resolution SEM image (as shown in Fig. 3.9(b)) indicated that copper nanoparticles were uniformly distributed on the surface of 3D printed anodes, forming even smaller pores with high density after electroless plating. These copper nanoparticles efficiently increased the specific surface area of 3D printed anodes, which would enable much more bacteria adhesion. However, the surface condition of copper mesh turned out to be quite smooth. Pores and other defects that can prompt bacterial growth were seldom observed but lots of wrinkles could be characterized when we increased the SEM resolution to 6k (Fig. 39(c) (d)). This means less space could be provided for bacteria to grow on, and thus the low power generation from MFCs with copper mesh anodes was expectable. Carbon cloth anode was also characterized by SEM before MFC operation. As the carbon cloth used for electrode fabrication is woven with carbon fibers, this feature was clearly demonstrated in SEM images of the surface. In Figure 3.9 (e), a bunch of carbon fibers was imaged with spacing between each carbon fiber. The MSDS sheet provided together with the carbon cloth indicated that a porosity of 80% was achieved for this carbon cloth, making it an ideal material for MFC anodes. However, the diameter of the carbon fibers were about several microns and there were few pores observed along the carbon fiber, which limits its potential to further increase the porosity and its performance in MFCs.
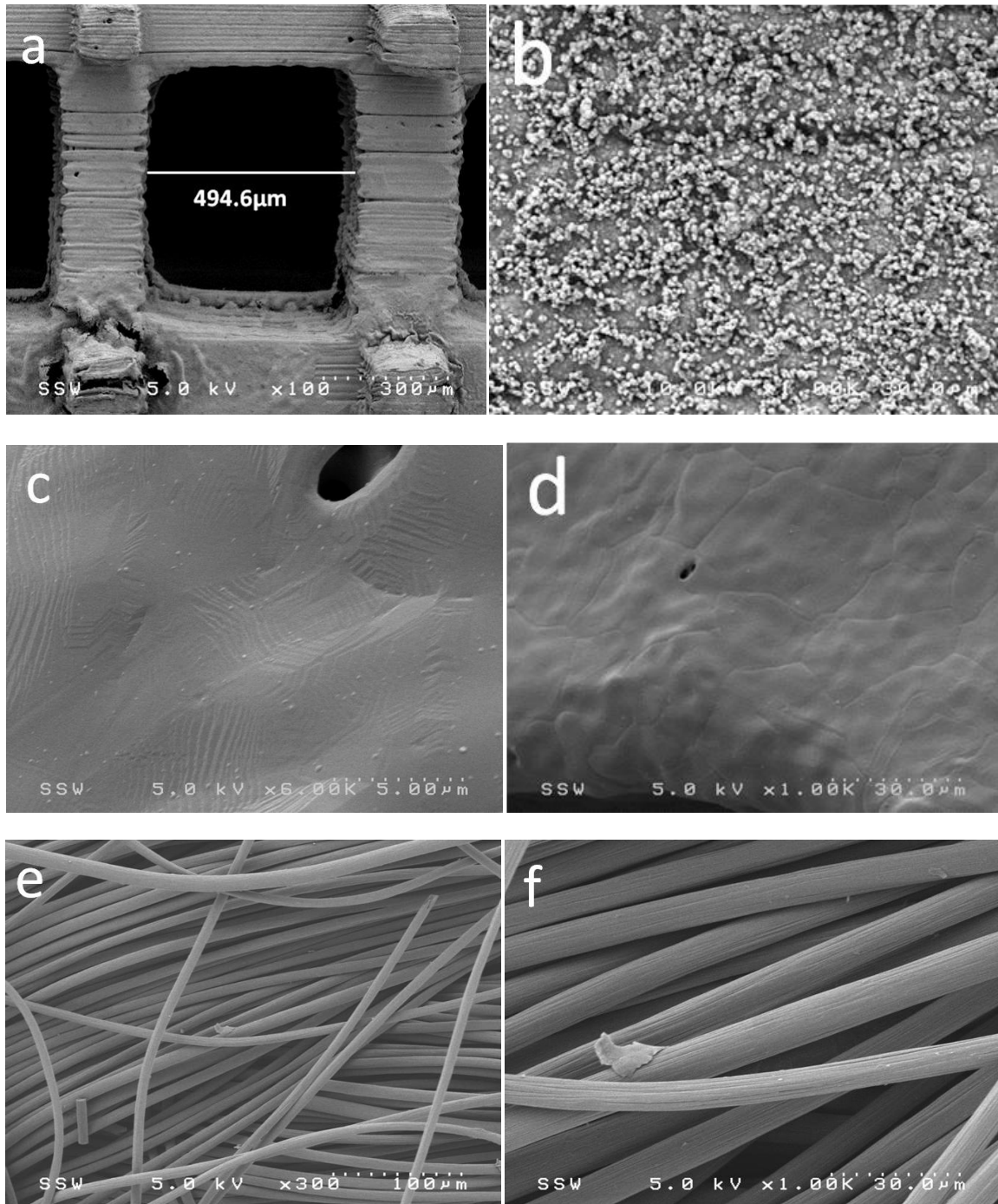
Figure 3.9: SEM image of (a) 3D printed porous anode with copper coated to the surface, (b) copper particles coated on 3D printed structure, and (c) (d) surface condition of copper mesh anode. (e) (f) presented the microstructures of the woven carbon cloth anode.

Though 3D printed anodes exhibited higher surface area, both of these two copper anodes were thought to be corroded during MFC operation, which led to the production of copper ions in solution. As we all know, copper ions are harmful for cell growth and can kill bacterial cells when they reach certain concentration. This might be the reason why lower power densities were reached for copper anodes compared with MFC with carbon cloth anode afterward. The high voltage generated in first cycle of MFCs with copper anodes was abnormal as it usually takes about 10 to 15 days for MR-1 to accumulate on the anodes and produce electrons and H^+. So we made an assumption that copper anodes were easily corroded during the first several cycles and thus chemical currents were produced from MFCs with copper anodes, which was confirmed later by ICP-MS and EDX analysis.

For ICP-MS analysis, 5 ml solution was taken out of the chamber of MFC with 3D printed anode during the first several cycles, 12 hours and 24 hours after MR-1 being fed, respectively. After centrifugation and autoclave, the solution was ready to do ICP-MS analysis. 732 μg/L copper ions were detected in the 12 hour solution while for the 24 hour solution the concentration of copper ions was 878 μg/L (as shown in Table 3.1). As there were no copper ions in the medium served into MFCs, the copper ions detected came from nowhere but the 3D printed anodes. As stated above, soluble copper is toxic to bacteria, this test result indicated that high voltages generated during the first several circles were probably due to the copper corrosion and bacterial growth might be restrained on Cu anodes. The restrained bacteria growth was proved by FESEM images below and resulted in low power outputs from MFCs with 3D printed anode and copper mesh anode.

Table 3.1: ICP-MS analytical results of 3D printed porous copper anode

Sample Identification *Parameter-mass ions*		MRL (µg/L)	12 h (µg/L)	24 h (µg/L)	STD @ 50 µg/L as %	STD@ 100 µg/L as %	STD@ 500 µg/L as %
Mg	24	5	3210	3680	107	118	110
P	31	50	315,000	382,000	103	110	107
K	39	10	181,000	291,000	110	119	108
Ca	40	10	480	872	132	133	112
Cu	64	0.1	732	878	114	123	112

Apart from ICP-MS, EDX analysis of the 3D printed anode with copper coating was also done before and after 40 days of MFC operation (Fig. 3.10 (a), (b)). The samples were carefully washed and dried before test. The EDX spectrum recorded from copper coating before MFC experiment showed very strong signal of copper element with an 84.7 weight percentage, indicating a very good electroless plating before MFC construction, while after taken back from MFC operation, only 62.3 wt % of copper was detected on the surface of 3D printed anode with a large increase in carbon and oxygen content. The corrosion of copper coating on the surface of 3D printed structures during MFC operation was proved again with this analysis. Two pictures of 3D printed anode before and after MFC running were also presented here (Fig. 3.10 (c), (d)). The copper anode looked darker after MFC operation, indicating possible copper corrosion during MFC power generation. Also shown was the thickness of copper coating after deposition onto the anode surface (Fig. 3.10 (e)). It's essential to measure the thickness of the copper layer, to determine the acceleration voltage needed for EDX analysis. ~2 µm thick copper layer can endure the bombardment of electrons accelerated by 15kV voltage without damage.
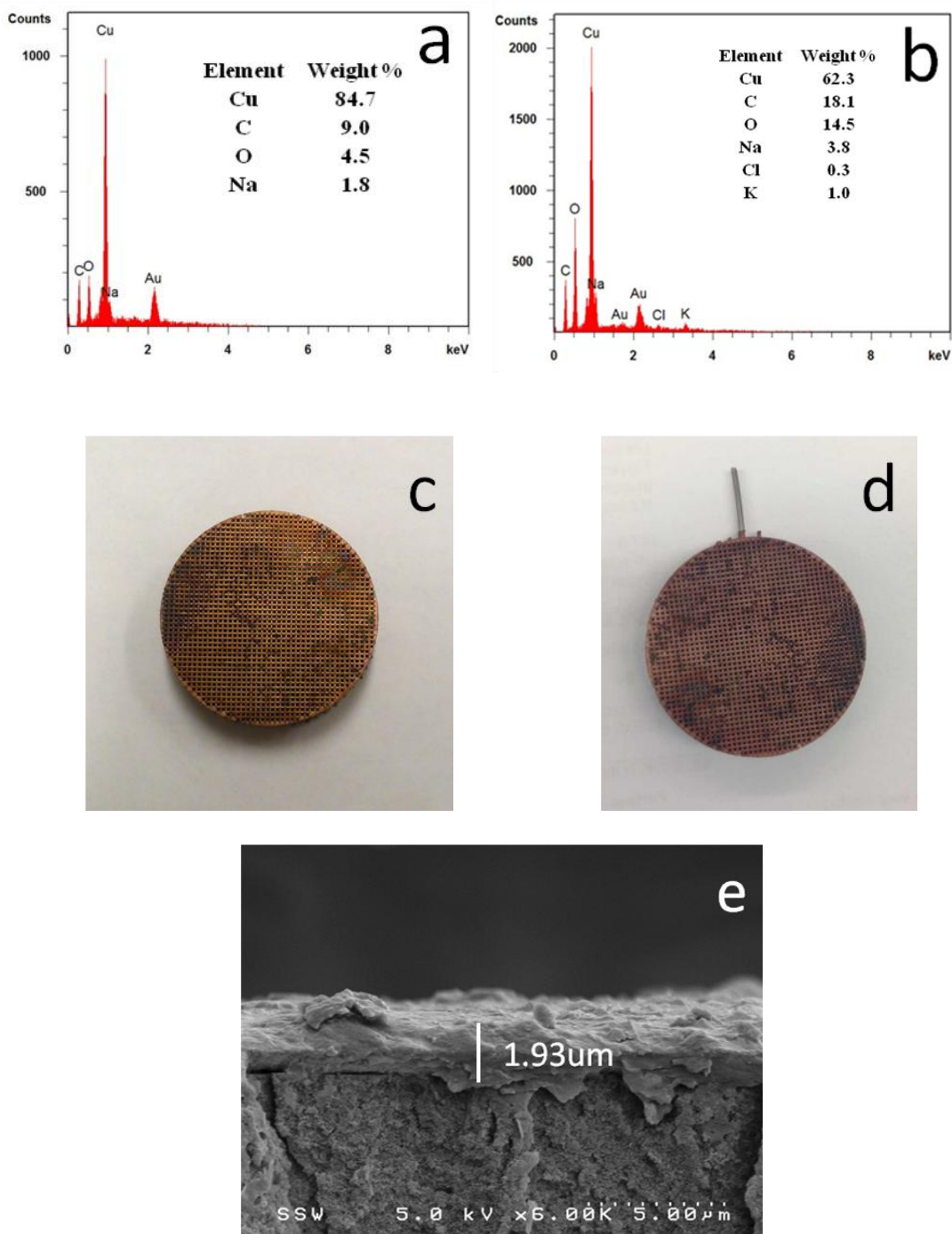
Figure 3.10 EDX analysis of 3D printed anodes with coated copper layers (a) before and (b) after 40 days of MFC operation. Picture (c) and (d) showed the same 3D printed copper anode before and after MFC operation, respectively. (e) The cross section of coated copper layer.

In order to investigate the impact of soluble copper on bacterial growth on MFC anodes, FESEM was further used to observe the formation of biofilm on the anodes after 40 days of MFC operation. We found that the biofilm grown on the carbon cloth anode was the thickest among that on all three anodes (Fig. 3.11). Layers of MR-1 biofilm were formed on the surface of carbon cloth anode, demonstrating a better biocompatibility of carbon materials. This also explains the much better performance of MFCs with carbon cloth anodes. But when we compared the biofilm formation on the two copper anodes, a much larger number of MR-1 cells were immobilized on the 3D printed anode with copper coating (as shown in Fig. 3.11 (a), (b), (c)). Lots of long MR-1 cells and extracellular polymeric substances were found growing and connecting to each other across the pores located at the outer (Fig. 3.11 (a)) and internal (Fig. 3.11 (b)) anode surface. As chance is larger for bacteria grow on outer porous layer to get organism for food, there were more bacteria adhering to outer porous layers than inner ones. However, when we looked at the surface of copper mesh anode, bacterial biofilm could be scarcely found except for some isolated bacteria (Fig. 3.11 (c)). As stated in Chapter 2, the power output of MFCs mainly depends on the electron transfer between anodes and bacterial biofilm. In this situation, we could barely expect high voltage and power density from MFCs with copper mesh anodes. So far, with these SEM images showing bacterial biofilm formation on three kinds of anode structures and results of the ICP-MS and EDX tests discussed above, we evidently proved the copper corrosion of 3D printed porous anode occurred during MFC operation and hindered the bacterial growth onto the surface of the porous anode. But 3D printed anodes exhibited a higher porosity, better biofilm formation, and electrochemical performances compared with copper mesh anode.
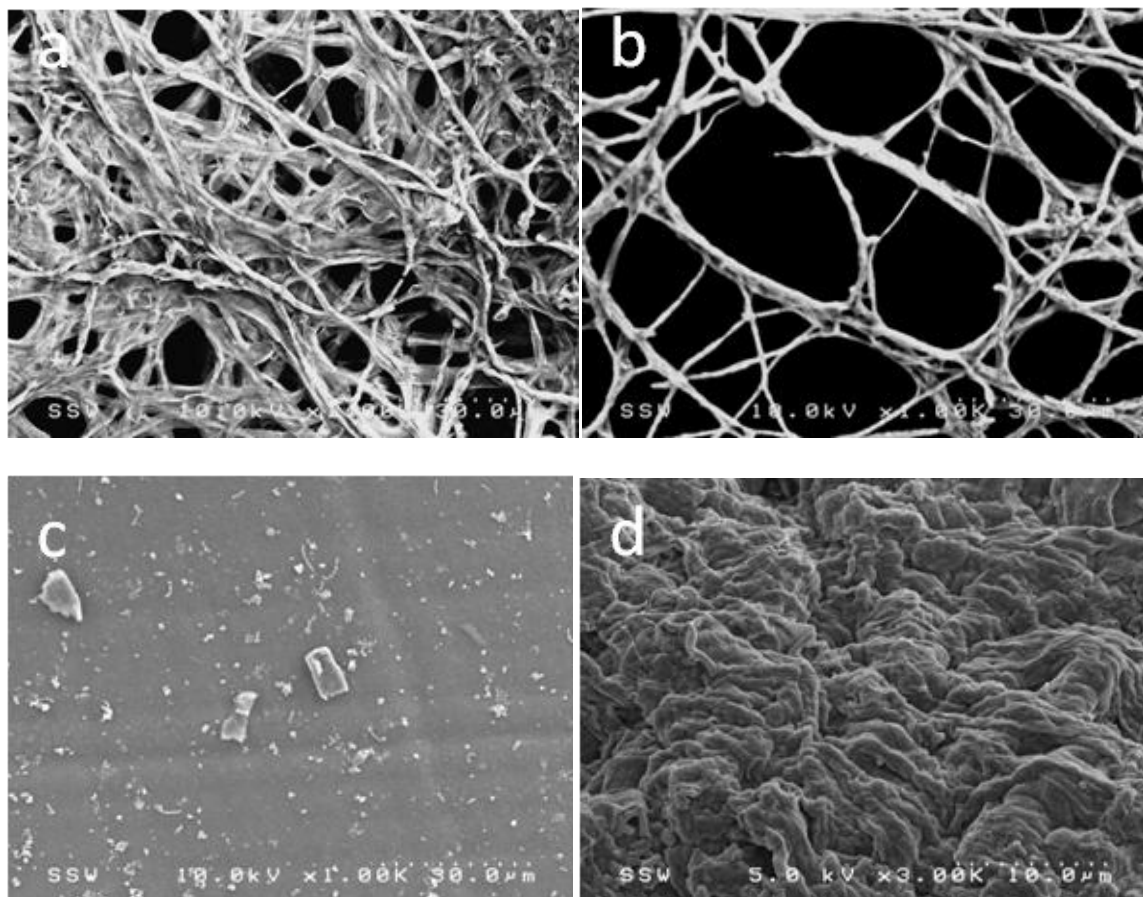
Figure 3.11 FESEM images of Shewanella MR-1 biofilms formed on MFC anodes after 40 days of operation. (a) top porous surface, (b) internal pore surface of 3D printed anodes, (c) surface of copper mesh, and (d) carbon cloth surface.

3.4   Conclusion

In this chapter, 3D printing technique was used to fabricate the 3D porous structure, followed by copper electroless plating. This 3D porous copper structure served as a new anode and was applied for the first time to an air-cathode MFC. The performance of this anode was compared to another two kinds of anodes, copper mesh and carbon cloth. The results showed that the 3D printed porous copper anode had larger surface area, more

bacterial adhesion and thus better electricity output compared with the copper mesh anode. So we could draw a conclusion that 3D printing is a promising technique that can be used to fabricate electrodes with tunable pore sizes in MFCs. But due to the copper corrosion during MFC operation, copper anodes exhibited much lower power output and less bacteria growth than the carbon cloth anode, which indicated the poor bio-compatibility of copper anodes. So here we suggest that 3D printed electrodes with high porosity and non-corrosive property be used in MFCs, such as carbon porous anodes. This conclusion led to our extensive research on 3D printed porous carbon anodes in Chapter 4.

Chapter 4

4   Fabrication of 3D Printed Porous Carbon Anode and its Application in MFCs

At the end of last chapter, we drew a conclusion that 3D printing technology was promising in micro porous anode structure fabrication but copper coating exhibited poor bio-compatibility compared to carbon materials. In this chapter, a different anode preparation method is adopted. First a brief introduction to polymer carbonization is given, followed by a detailed description of the preparation procedure of 3D printed structures with different pore sizes. These porous structures are carbonized before serving as anodes for MFCs. After MFC construction, several testing techniques are discussed, including voltage measurement, linear sweep voltammetry, and electrochemical impedance spectroscopy. Biofilm characterization is presented at last to help explain the different performance of MFCs.

4.1   Introduction

Carbonization of polymers is a thermochemical treatment process with a long history. The first application of this technique started with the determination of the composition of coal. One popular trend in coal chemistry was the study about thermal treatment, which would change the composition and structure of the coal.[105] As polymers usually forms the main part of a coal, the transformation of polymers are of great significance during thermal process. From the chemical and physical point of view, numerous thermophysical and thermochemical reactions occur during coal treatment. Lots of researches have demonstrated that destruction and structuring of different polymers exist

all the time during heat treatment. [106,107] What determines whether the polymers will be burnt into ash or be converted to carbon saturated products are the heating conditions and the atmosphere. With special treatment, a majority of polymers forming the coal can be converted to carbon products, from which carbon materials and fuel resources are formed and then used in different aspects of industry.

The increasing demand for energy and fossil fuel consumption rates have set higher requirements for energy exploitation and accelerated the research on sustainable energy technologies. [108,109] Energy conversion from sustainable resources and wastes from life and industry is one main method to achieve this. MFCs are thought to be one of the most promising energy conversion technologies due to their application in wastewater treatment.[110] However the lower power density still limits the commercialization and scaling up of MFCs. Carbon-based materials such as carbon cloth, graphite plate, carbon brushes, CNTs and graphene have been tested for MFC electrodes as stated in Chapter 2. Even though composite materials made of conductive polymers and graphene or CNTs have shown excellent performance in MFCs, the high cost and complicated fabrication processes of these materials make it difficult for MFC to scale up compared to the carbon porous structures. Besides, the charge storage property of these materials is affected by the lack of porous structure and lower practical surface area.[111] For further improvement, preparation of highly porous carbon materials has been achieved either by alkaline activation or by templated methods, which still require complex synthesis procedures.[112] Therefore, novel approaches to fabricate high surface area carbon materials with controllable porosity are yet to be discovered.

Direct carbonization of polymers probably is the most facile and promising approach for the porous carbon material preparation. However, only a limited number of reports have been published on the fabrication of carbon materials with high porosity by direct pyrolysis, without any extra processes or external agents.[113] Polymers are ideal precursors that could be changed into porous carbon materials by carbonization. Polyacrylonitrile (PAN) is one of the most commonly utilized polymers for carbonization. Co-polymer of PAN and poly(n-butyl acrylate) (PBA) was reported by Zhong et al.[114] to produce porous carbon structures and a surface area of $500 m^2\ g^{-1}$ was obtained after carbonization without any activation. Three dimensional carbon nano or micro structures such as graphene aerogels have attracted much attention as anode materials for MFCs due to their wide pore size distribution, ranging from macropores, mesopores to micropores.[115] Until now very few reports have been released on the fabrication of 3D carbon structures by direct carbonization. In this chapter, we report an easy approach to prepare microporous carbon structures through 3D printing, followed by direct carbonization of UV curable resin. Different cross-linking polymer resins are tested and no activation is required to achieve conducting and porous carbon anodes except high temperature pyrolysis. Excellent MFC performances can be anticipated.

4.2 Experiment

4.2.1 3D printed carbon anode preparation

The preparation of 3D porous carbon anodes started with the printing of 3D anode structures, same as the procedure described in Chapter 3. But this time, different specific pore sizes of anode matrixes were designed for printing, ranging from $100\,\mu m$ to $500\,\mu m$,

to test the effect of pore sizes on MFC performance. The pyrolysis property of two different types of UV curable resins (Asiga PlasClear and Miicraft Clear 2005T) was tested after solidification. As the size shrinkage usually goes with polymer carbonization, several samples printed with the two resins were employed to measure the shrinkage ratio before we finally confirmed the design (Fig. 4.1 (a)). According to the measured shrinkage ratio (original diameter: diameter after carbonization= 2.3:1), anode structures were redesigned to ensure that anodes with different pore sizes had same dimensions with 3D printed copper anode in Chapter 3(2.75cm$\times$2.75cm$\times$0.5cm) (shown in Fig. 4.1 (b)).
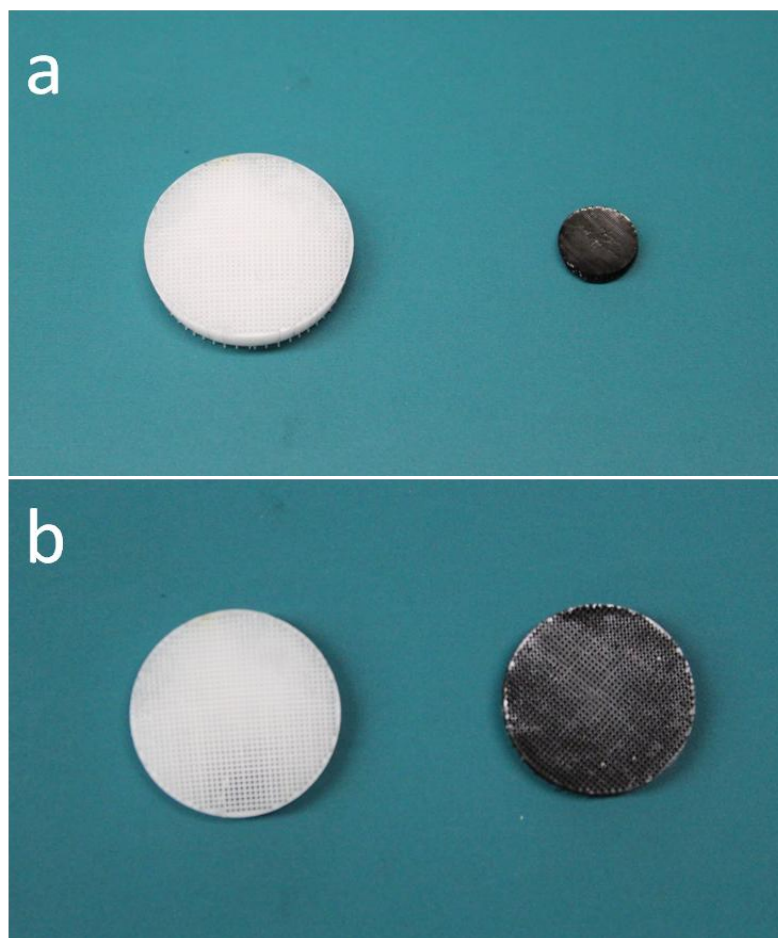
Figure 4.1: Comparison of original and carbonized 3D printed anode structures (a) before and (b) after redesigning.

After designing, 3D porous structures were ready for printing. As two different types of resins were used, different printing parameters were developed for each resin. For PlasClear resin purchased from Asiga, the same parameters used in copper porous anode printing were utilized, with a layer thickness of 25 μm, burn-in and normal exposure time of 1 second, respectively. And for Clear 2005T resin from Miicraft, the 3D porous matrixes were also printed out with a slice thickness of 25 μm. The burn-in exposure time and normal exposure time were 5 seconds and 0.5 seconds, respectively. And the number of burn-in layers was six every cycle. The platform of the 3D printer was cleaned with pure alcohol and then washed 3 times with DI water. It was blow-dried before it was located back to the 3D printer.

Figure 4.2: Lindberg/Blue M Furnace purchased from Thermo Scientific. Pure nitrogen gas was pumped in during carbonization

After the anode structures were printed out with the two resins, they were treated by sonification in ethanol for 10 min. The substrates were washed 3 times by DI water before air dry. The samples were then placed in a quartz boat and sent into a tube furnace (Lindberg/Blue M, Thermo Scientific) for carbonization (Fig. 4.2). Nitrogen gas was pumped into the quartz tube before heating. And different heating rates were set for cured polymer carbonization at different stages as shown in Table 4.1. During the carbonization and cooling period, nitrogen gas was pumped at a flow rate of 3L/min.

Table 4.1: Different parameters used in cured polymer carbonization.

Test	25-350℃	350-450℃	450-800℃
1	3℃/min	0.4℃/min	2℃/min
2	3℃/min	1℃/min	2℃/min

After carbonization, 3D structures printed from different resins were compared with each other. The results turned out to be very surprising as no structures remained standing in the quartz boat for 3D matrixes printed using Asiga resin while 3D porous structures made from Miicraft resin excellently kept their porous lattice feature. However, the different heating rates around the solidifying point made the samples printed with Miicraft resin bore different thermal stresses and thus presented different shapes (as shown in Fig. 4.3). The carbon porous structure in Figure 4.3 (b) was carbonized at a slow heating rate of 1℃/min, in which situation more thermal stress was taken by the sample and the matrix bending was thus caused by uneven stress.
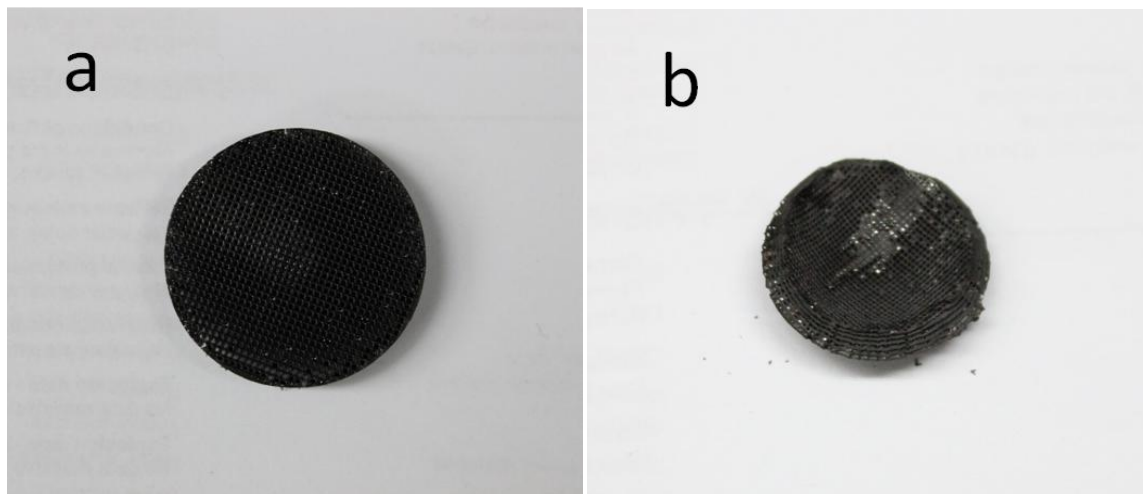
Figure 4.3: 3D porous structures printed using Miicraft resin were carbonized at different heating rates around the solidifying point (a) 0.4℃/min and (b) 1℃/min.

As for 3D matrixes printed using Asiga resin, nothing was left except some charcoal ash. The carbon yields were measured by thermal gravimetric analysis (High Temp DTA/TGA Rheometer, TA Instruments) for both PlasClear resin and Miicraft resin. TGA is a method of thermal analysis of physical and chemical properties of materials as a function of increasing temperature. Lots of information can be provided by TGA, such as phase transitions, including vaporization, adsorption, and desorption. Besides, TGA can provide information about chemical changes including decomposition and oxidation.[116]

TGA is often employed to determine certain characteristics of materials that show mass loss or gain due to reactions such as decomposition and oxidation. In this study, TGA was used to analyze the decomposition patterns of cured resins and determine the carbon yields of the two resins. In Fig. 4.4, the mass percentages of two resins were measured as a function of increasing temperature. The PlasClear resin from Asiga exhibited a sharp mass loss at the temperature range from 350 to 450℃, leaving only 2.4 wt% carbon at the

temperature of 500℃ and 1.5 wt% carbon at the end of the experiment. Likewise, a sharp

drop in mass percentage was also observed for Miicraft resin, but the carbon yield at 500℃

was about 8.5 wt% and 7.1 wt% carbon remained at last, which was enough for the

matrix itself to keep the lattice structure and support its own weight. So we chose

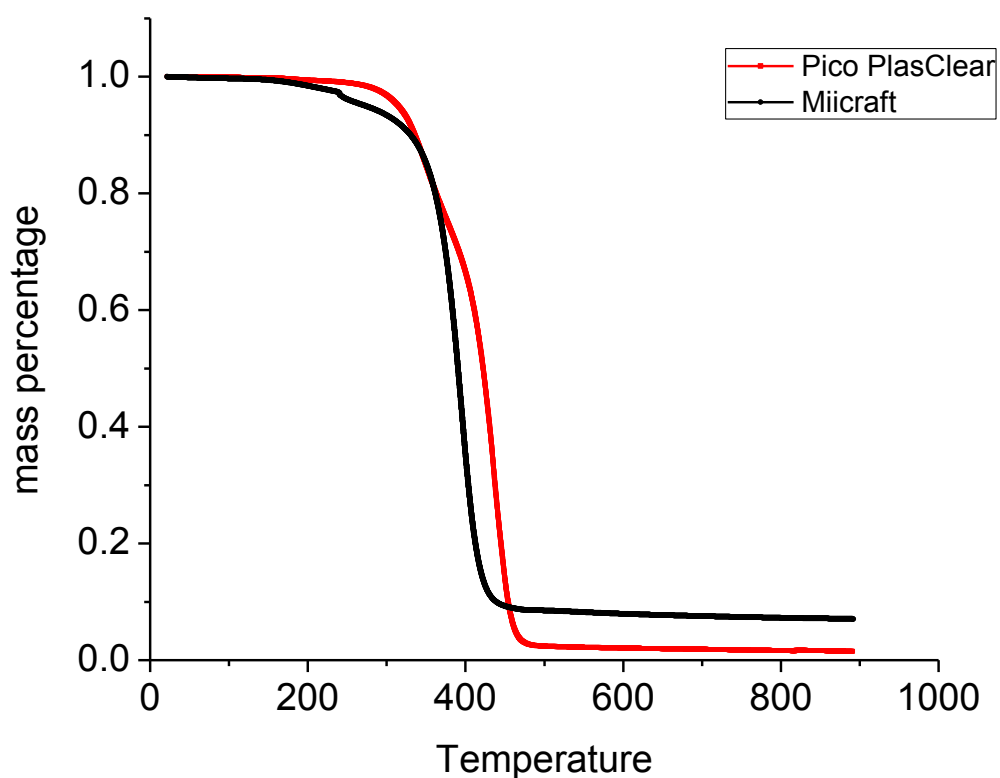Miicraft resin for 3D carbon porous anodes printing afterward.

Figure 4.4: TGA analysis of the PlasClear resin and the Miicraft resin as a function

of increasing temperature. The red line represented mass percentage of the

PlasClear resin while the black showed the mass change of Miicraft resin. The unit

of the temperature is ℃.

4.2.2   **Shewanella oneidensis MR-1 cultivation**

Shewanella oneidensis MR-1 was cultivated aerobically in the same way as stated in Chapter 3. The agitation was 150 rpm and the temperature was kept at 30 ℃. TSB medium was used and after centrifugation and cell wash for three times with PBS buffer, the bacteria were inoculated into another growth medium with 18mM lactate, also same as reported in Chapter 3. The bacterial cell densities were measured at 600nm with the UV/Vis spectrophotometer. Before bacterial inoculation into MFCs, it took about 3 days for the cell densities to reach 0.4 at 600nm.

4.2.3   **MFC construction and setup**

The same configuration of MFC chambers was adopted for carbon porous anodes. Air-cathode MFC chambers of 4cm long and 3cm in diameter were used for MFCs with 3D printed carbon anodes. The pore sizes of each anode were different, from $100\,\mu m$, $200\,\mu m$, $300\,\mu m$, $400\,\mu m$ to $500\,\mu m$, and the dimensions of anodes are same ($2.75cm \times 2.75cm \times 0.5cm$). The air-cathode was a gas diffusion layer ($7\ cm^2$) made from carbon cloth and coated with 0.5 mg/cm^2 of Pt (Fuel Cells Etc). The spacing between the anode and the air-cathode was 2cm (Figure 4.5). All MFCs were sealed by epoxy and dried before use.

Five air-cathode MFCs were constructed with the 3D printed carbon porous anodes fabricated above and the carbon cloth anode was chosen for MFC performance comparison. All components were autoclaved before bacteria inoculation. The growth medium prepared above served as substrate in MFCs and mixed with bacterial culture for inoculation. After adding lactate, the medium is adjusted to pH 7 using 2M HCl.
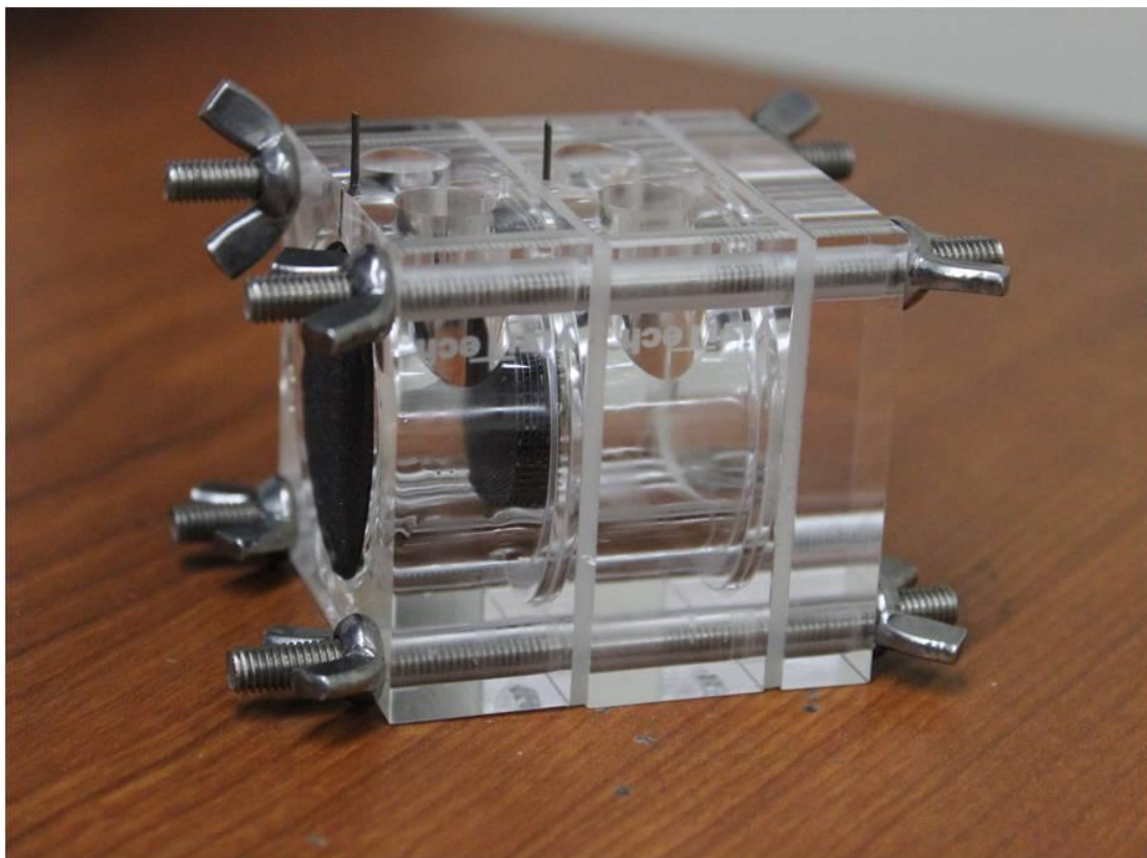
Figure 4.5: Air-cathode MFC with 3D printed carbon porous anode. The chamber was sealed by epoxy.

MFCs were inoculated with 50% inoculum of S. oneidensis MR-1 and medium. All MFCs were connected to a 1000Ω external resistor. The solution in MFCs was replaced every 2.5 days until MFCs produced relatively stable voltages and then only fresh medium was added over the following fed batch cycles. Medium replacement was conducted in a laminar flow hood (Forma Class II, Biological Safety Cabinet, Thermo Scientific). All the six MFCs were operated at room temperatures ($20\pm2\,^{\circ}\!C$). The MFCs were ready for testing and considered enriched once they achieved similar maximum voltage for four consecutive batch cycles (about 15 days for air-cathode MFCs).

4.2.4   Characterization

(1) Voltage

The same voltage monitor system introduced in Chapter 3 was used in voltage measurement here. The cell voltages across a 1000 Ω external resistor was recorded every 5 min using a high –resolution DAQ device (USB 6251 BNC, National Instrument) and the LabVIEW software package (National Instruments). Six data channels of DAQ were utilized for voltage measurement of all six MFCs and were controlled by LabVIEW program (Fig. 4.6).
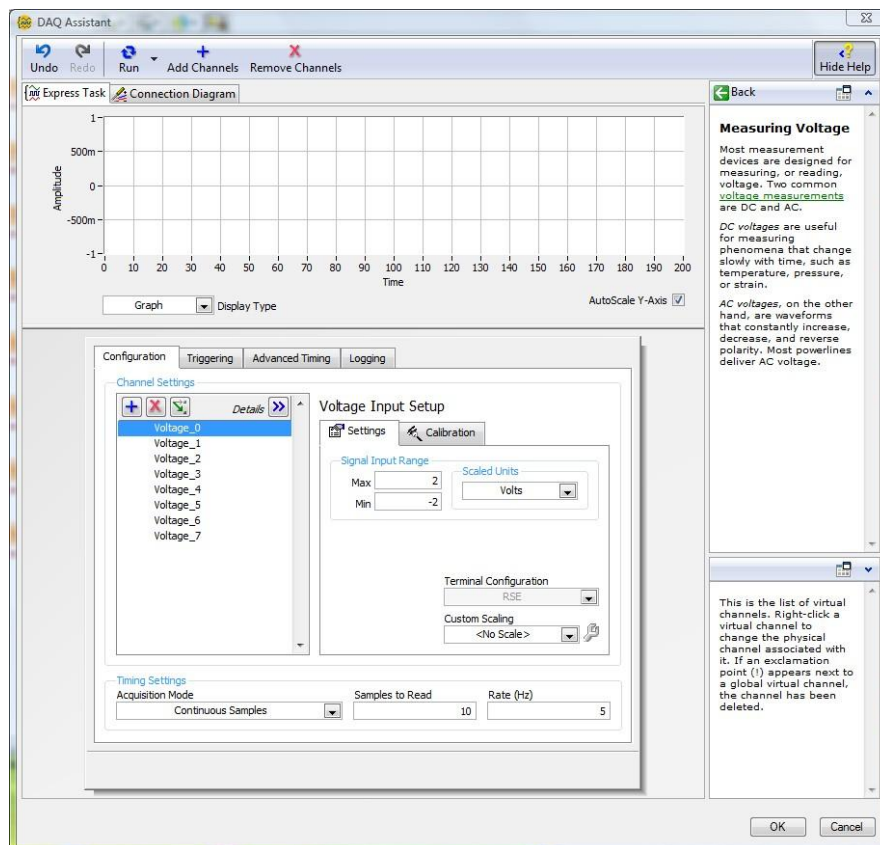

Figure 4.6: Eight data channels for voltage data acquisition added in DAQ Assistant, which enable the voltage monitor of eight MFCs at the same time.

(2) Linear sweep voltammetry (LSV)

Linear sweep voltammetry (LSV) was also conducted with a potentiostat (CHI 1200a, CH Instruments Inc.) to obtain polarization curves of MFCs. MFCs were kept at their open circuit potentials (OCP) for 40 minutes to stabilize, and then scanned from OCP to 0 mV at a rate of 0.1mV/s, with the anode serving as working electrode and cathode serving as the counter and reference electrode. Power densities were calculated using Equation 2-4 based on the anode projected surface area (6 cm^2) and plotted as a function of increasing current densities. The peak power densities for MFCs with different anodes always fall at the middle of the scanning range.

(3) Electrochemical impedance spectroscopy (EIS)

Electrochemical impedance spectroscopy (EIS) was conducted to determine the performance of 3D printed carbon porous anodes, especially the electrode resistance in chemical solution. To do EIS measurement, a small amplitude alternating potential should be applied to the electrochemical systems, and the ratio of the alternating potential and the current is the impedance of the systems, which changes with the frequency of the sine wave[117]. The EIS could be used to analyze the electrochemical kinetics of electrodes, electric double layers, and diffusion. Electrode materials, electrolyte and corrosion could be also studied using EIS data.

In this thesis, the EIS measurement was carried out with a multi-potentiostats (VMP3, Biologic) using an impedance-potential technique under whole cell conditions (Fig. 4.7). The measurements were conducted in a dual-electrode mode by testing the impedance spectra of MFC anodes as working electrode while the cathode served as a counter and

reference electrode. A sine wave of 5mV was applied to each MFC system when collecting impedance spectra at the open-circuit potential, with a frequency range from 100 kHz to 10 mHz. The data collected were analyzed and fitted with an equivalent circuit using Zview software. The MFC configurations, the solution and the cathode materials of MFCs were all the same, and all six MFCs were kept at open circuit for 40 min before EIS measurements.

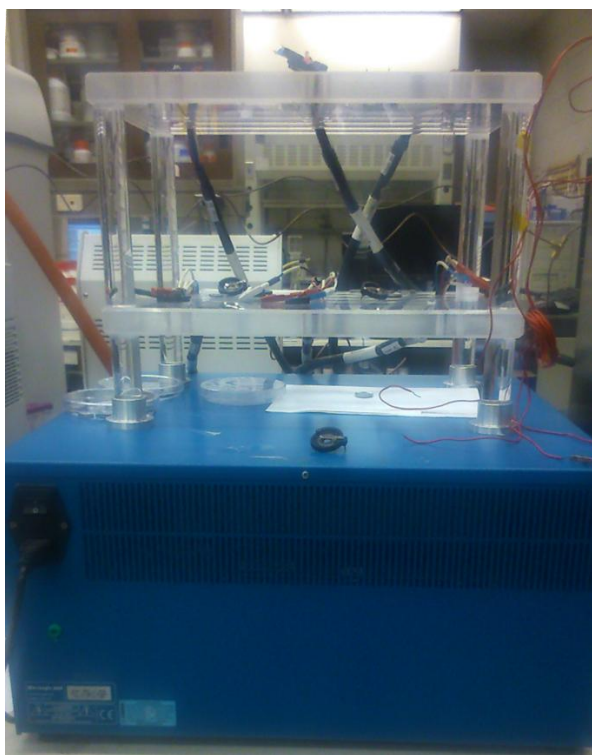**Figure 4.7: Multi-potentiostat (VMP3) used for EIS measurement.**

(4) SEM biofilm characterization

After completing various measurements and tests of each MFC, the anode structures were taken out of MFCs chambers and examined by scanning electron microscopy (SEM). Same procedures were taken to preserve the certain morphology of biological samples in some certain environments and enhance the imaging quality.

After all six anodes were taken out of MFC chambers, SEM was used for assessing whether bacterial bioflim was formed on the surface of top layers or inner layers of porous carbon anodes. Anodes with potential bacterial biofilm were first washed three times in pH 7 PBS to remove organism remained and then chemically fixed with 3% glutaraldehyde. The samples in the glutaraldehyde were kept in a refrigerator overnight at 4℃. After that, the bacterial biofilm on anodes was again rinsed softly in pH 7 PBS, and then diluted PBS (1:1 with distilled water) and DI water. A graduated series of ethanol solution with increasing concentrations (20%, 40%, 60%, 80% and 100%) were utilized to dehydrate the anodes. After rinsing in 100% ethanol for three times, the specimen were dried in a vacuum chamber. Following the dehydration of bacterial biofilm, samples were deposited with a thin layer of gold in a sputtering coating chamber and examined on a Hitachi S-4500 field emission SEM with a Quartz PCI XOne SSD X-ray analyzer.

4.3 Results and Discussion

MFCs with 3D printed carbon porous anodes were operated more than 40 days until stable voltages were monitored for several consecutive cycles. After stabilization, the voltage generated by each MFC remained at a relatively constant maximum value and dropped quickly at the end of each cycle. The voltages of all MFCs jumped back to the maximum values within hours (usually less than 1.5 hours) upon replacement of the solution in the MFCs with fresh lactate medium. At the first two cycles, all MFCs including the one with a carbon cloth anode produced similar but pretty low voltages. However, after about 20 days' operation, maximum voltage disparity occurred among all MFCs (Figure 4.8). The carbon porous anode with a pore size of 300 μm produced the

largest maximum voltage 453.1±8.5 mV while only a voltage of 190±5 mV was achieved by the MFC with carbon cloth anode (as shown in Fig. 4.8 (c) (f)). Compared to the carbon cloth anode, all MFCs with 3D printed carbon porous anodes produced much higher maximum voltages. 3D carbon anodes with 200 μm pores and 300 μm pores even achieved maximum voltages more than two times that of carbon cloth anode, which exhibited the great advantage of 3D printed carbon porous anodes over the plain carbon cloth anode. Moreover, compared to the MFC with a carbon brush anode reported by Valerie Watson et al.[118], the voltages generated by 3D carbon porous anodes exhibited even larger values, demonstrating the promising application of 3D printed carbon structures in MFCs. To better compare the performance of different carbon anodes, the maximum voltages generated by each MFC were listed in Table 4.2.

Table 4.2: Maximum voltages produced by different MFC anodes.

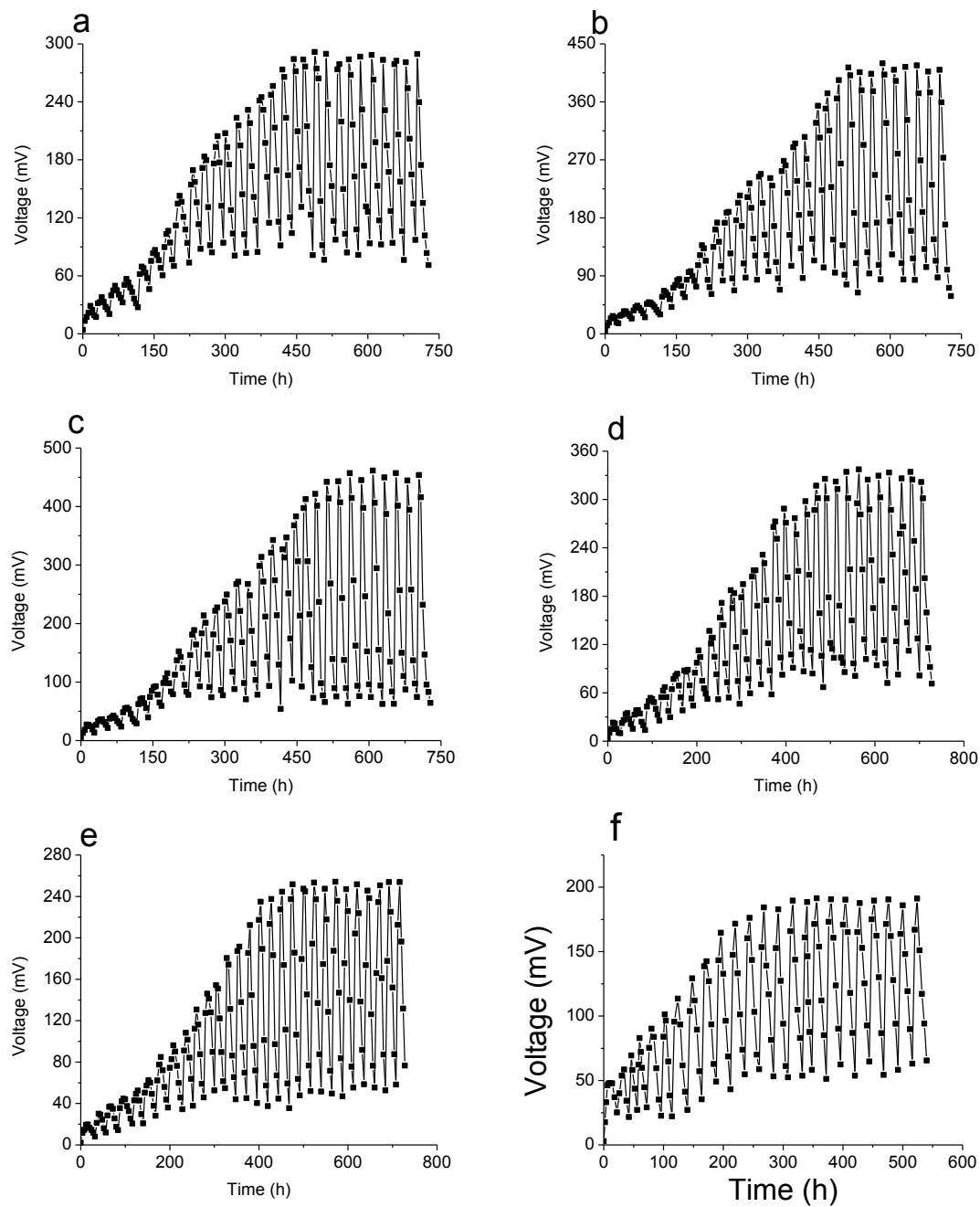| Anode Structure	Pore Size/μm	Maximum Voltage/mV
3D printed carbon porous anode	100	285.4±6.3
	200	411.7±8.1
	300	453.1±8.5
	400	329.5±7.9
	500	249.3±4.8
Carbon cloth anode	---	190±5

Figure 4.8: Voltage production of MFCs with 3D printed carbon anodes with pore sizes of (a) 100 μm, (b) 200 μm, (c) 300 μm, (d) 400 μm and (e) 500 μm. (f) represented the voltage produced by the MFC with a carbon cloth anode.

Polarization curves plotting voltage as a function of current were utilized to analyze and characterize MFC performances. In this chapter, the polarization curves of six MFCs were measured to evaluate the effect of the pore sizes of different anodes on anodic electrochemical behavior of MR-1. Dual-electrode mode was adopted in polarization curve measurement with different anodes serving as the working electrodes, and the reference and the counter electrodes were the Pt/C carbon cloth cathode. The polarization curves obtained were listed in Appendix A. And the open circuit potentials and maximum power densities for the six MFCs with different anodes were listed in Table 4.3. The OCPs produced by MFCs with 3D printed 200 μm, 300 μm, 400 μm and 500 μm pore-sized anodes were also larger than that by the MFC with a carbon brush anode.[14]

Table 4.3: Open circuit potentials and maximum power densities produced by different MFC anodes.

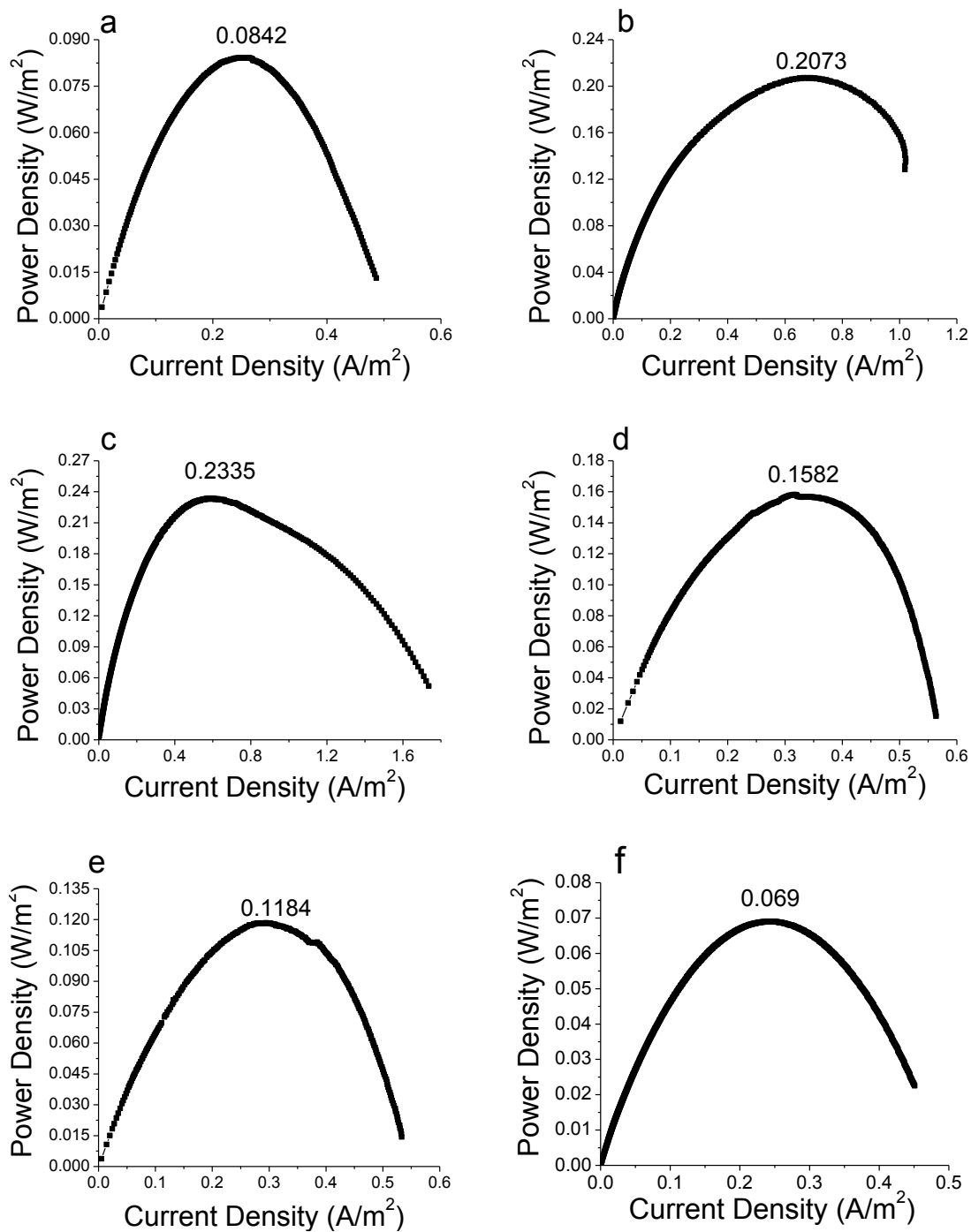| Anode Structure	Pore Size/μm	OCP/mV	Maximum Power Density/(mW/m^2)
3D printed carbon porous anode	100	664.2	84.2
	200	1206	207.3
	300	1263	233.5
	400	909.9	158.2
	500	761.4	118.4
Carbon cloth anode	---	673.0	69.0

Figure 4.9: The power density curves of MFCs with 3D printed 100 μm, 200 μm, 300 μm, 400 μm and 500 μm pore-sized anodes were plotted as (a), (b), (c), (d) and (e), respectively, based on the same projected surface area of anodes (6cm^2). For comparison, power density produced by the carbon cloth anode was plotted as (f).

The power densities of each MFC were calculated based on polarization curves and the projected surface area of anodes (6 cm^2). The maximum power densities generated by MFCs with 3D printed carbon porous anodes were listed in Table 4.3. Compared to 69.0 mW/m^2 for carbon cloth anode (as shown in Fig. 4.9 (f)), power densities generated by 3D carbon porous anodes were much larger. The anode with a pore size of 300 μm even produced a power density that was about 3.4 times larger than the carbon cloth anode, which again demonstrated the great potential of 3D printed carbon porous anodes in MFC. Logan's group reported a power output of 148±20 mWm^{-2} based on a carbon brush anode (with a porosity of 95% or more) of MR-1 inoculated MFCs. Compared with our results, the power density produced was still lower than those produced by 3D carbon anodes with pore sizes of 200 μm, 300 μm, and 400 μm. It was then obvious that 3D printed anodes could help enhance the power generation of MR-1 MFCs as the power densities for 3D printed anodes were larger than that of three dimensional carbon brush anode.

To further study the performances of 3D printed carbon porous anodes, the electrochemical impedance spectroscopy of the six anodes was conducted. The EIS of the six MFCs illustrated a semicircle, which indicated the internal resistance of the MFCs. In the EIS plots, the diameters of the semicircles equal to the charge transfer resistances of MFCs and the values of the first intersections in each plot with X-axis represent the solution resistances. For the diffusion resistance, it is determined from the low frequency response of the plot of the whole cell experiment. Although it was possible to use circle fit analysis for different resistances of the MFC cells, the values were determined by fitting equivalent circuits to data with Zview software. The Nyquist plots were presented as followed and fitting results were also given in Fig. 4.10.
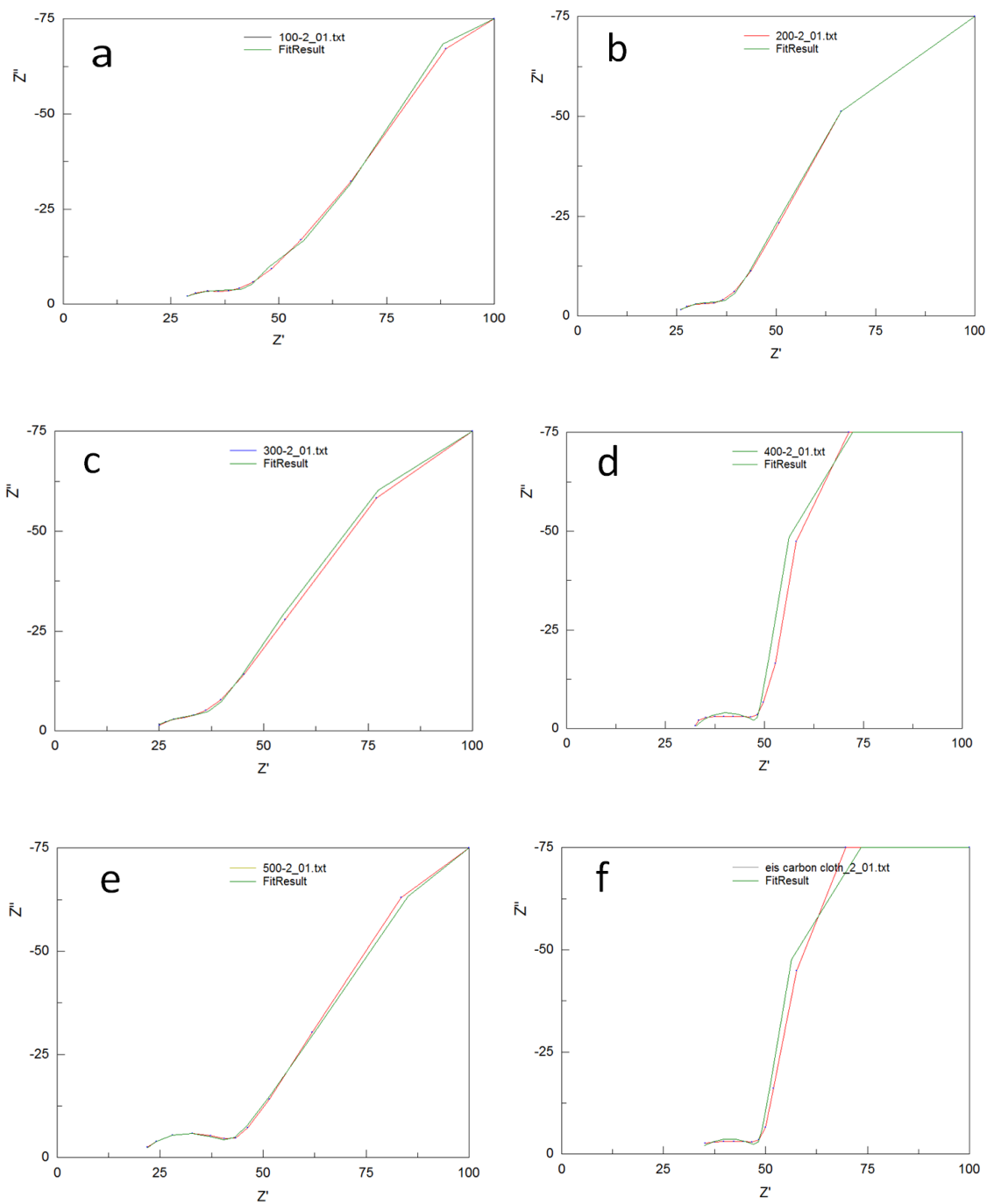
Figure 4.10: Nyquist plots of EIS data for different anode structures (red line), and equivalent circuit model fit (green line). Note that the circle fit provides excellent agreement with the data.
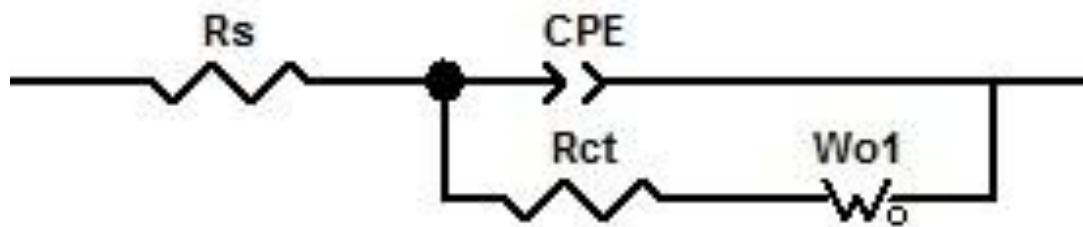
From Table 4.4 shown above, we could find that the solution resistance of MFCs with 3D printed carbon porous anodes was around 25Ω, which was about 8Ω lower compared to the MFC with carbon cloth anode, while the charge transfer resistance of the carbon cloth anode was lower than that of 3D printed carbon porous anodes (13.5Ω VS. 21Ω). The solution resistance and the charge transfer resistance measured were comparable to the amount measured using graphite fiber brush anode by Bin Wei et al.[119]. However, the solution resistance and the charge transfer resistance only accounted for part of the total internal resistance. The diffusion resistance could also affect the performance of MFCs. The Bode plots of EIS measurement of the six MFCs were shown in Appendix B to determine the diffusion resistance (R_d) of each MFC. As stated above, R_d could be determined from the low frequency response of the Bode plot. Bode plots present EIS data of the magnitude of impedance as a function of the log of the frequency of the applied AC signal. From the plots, we could find that the average diffusion resistance of 3D printed carbon porous anodes was about 370 Ω, which was far smaller than that of carbon cloth anode (1200 Ω). Overall, the average total resistance (R_t) of MFCs with 3D printed carbon porous anodes was about 410Ω, while for carbon cloth anode the R_t was about 3 times larger reaching 1250 Ω. The results obtained in this experiment were much lower than that reported by Zhen He et al. [120] and were comparable with the data published by Bin Wei et al.[15] using mixed culture. It was obvious that the porous structures assisted the diffusion process of MFCs.

To explore the reason why all 3D printed carbon porous anodes generated higher power densities than carbon cloth anode, we studied the surface condition of each MFC anode. SEM images in Fig. 4.12 (a) - (e) illustrated the well printed and carbonized 3D porous

anode structures, with precisely controlled pore sizes. These highly porous structures indicated more surface area for bacterial growth. The micro pores enabled good mass transfer and more bacterial adhesion into the inner layers of anodes, which was demonstrated by the diffusion resistance of the 3D porous anodes compared to the carbon cloth anode. Apart from the microporous structures, the high-resolution SEM images (as shown in Fig. 4.12 (g) - (k)) indicated that even smaller pores were formed after carbonization and were uniformly distributed on the surface of 3D printed anodes with high density. The smaller pores were about 2 to 5 μm in diameter, which were suitable for bacterial growth and adhesion onto as MR-1 bacterial cells are usually several microns long. The smaller pores located at the carbon rods efficiently increased the specific surface area of 3D printed anodes, which would further enhance the bacterial biofilm formation and increase MR-1 cell densities. As bacterial densities on the anodes play a significant role in electricity output, 3D printed porous anodes were expected to produce higher power densities, which were consistent with the results we got above. But when we looked at the surface of carbon cloth, elastic carbon fibers were found forming interspaces between each other. However, no smaller structures were discovered except that, which meant less space could be provided for bacteria to grow on, and thus the lower power generation from MFCs with carbon cloth anode was expectable. Though a porosity of 80% was achieved for this carbon cloth, the lack of even smaller structures, such as pores and voids, limited its potential to further increase its porosity and enhance the performance in MFCs serving as anode material. On the other hand, the EDX analysis of the carbonized porous anodes (Fig. 4.12 (l)) showed that 4.7 wt% nitrogen element was detected. As N-doped carbon materials were reported to have better electron transfer

efficiency[121] and electrocatalytic property[122], the 3D printed carbon anodes were thought to be more suitable for application in MFCs.
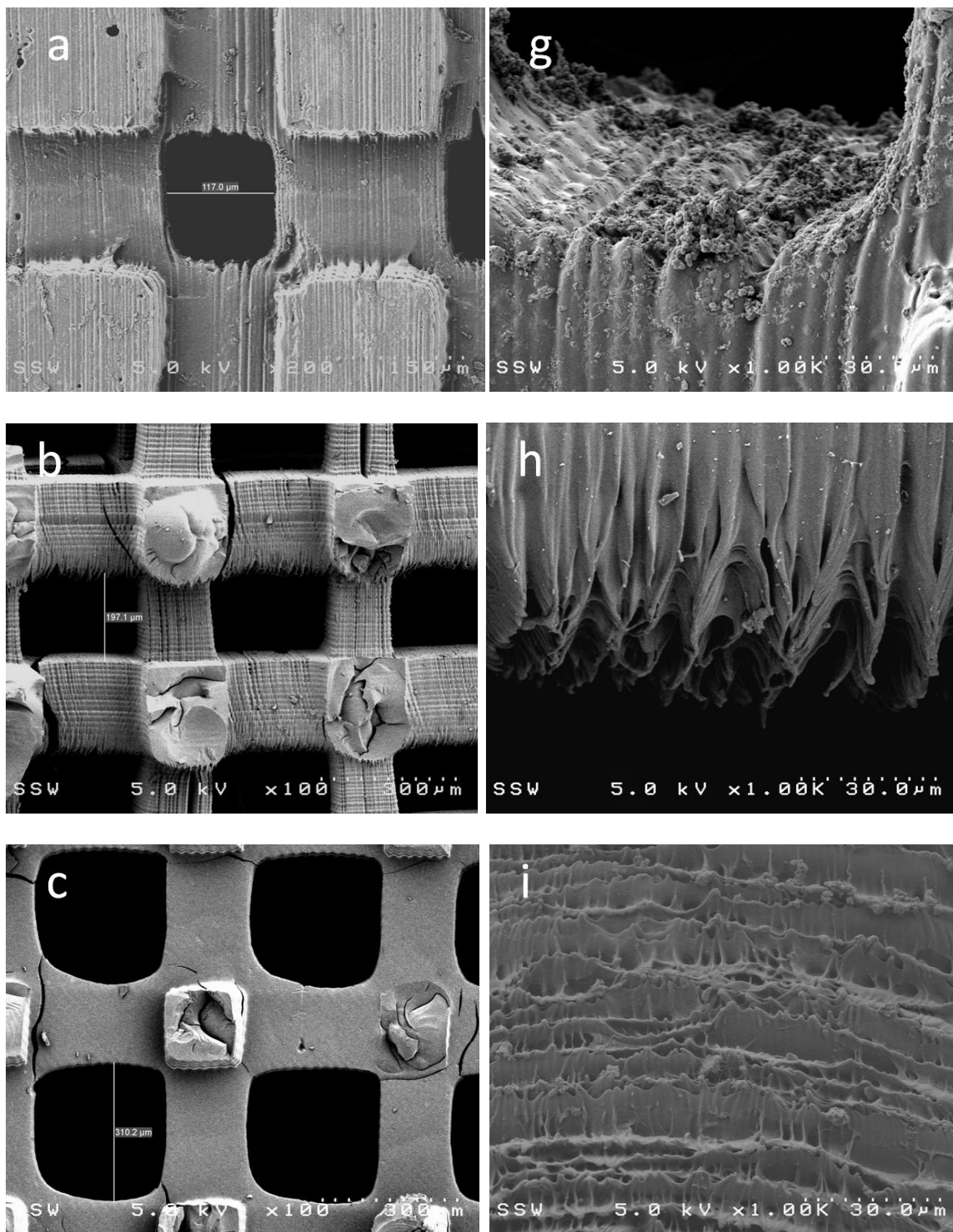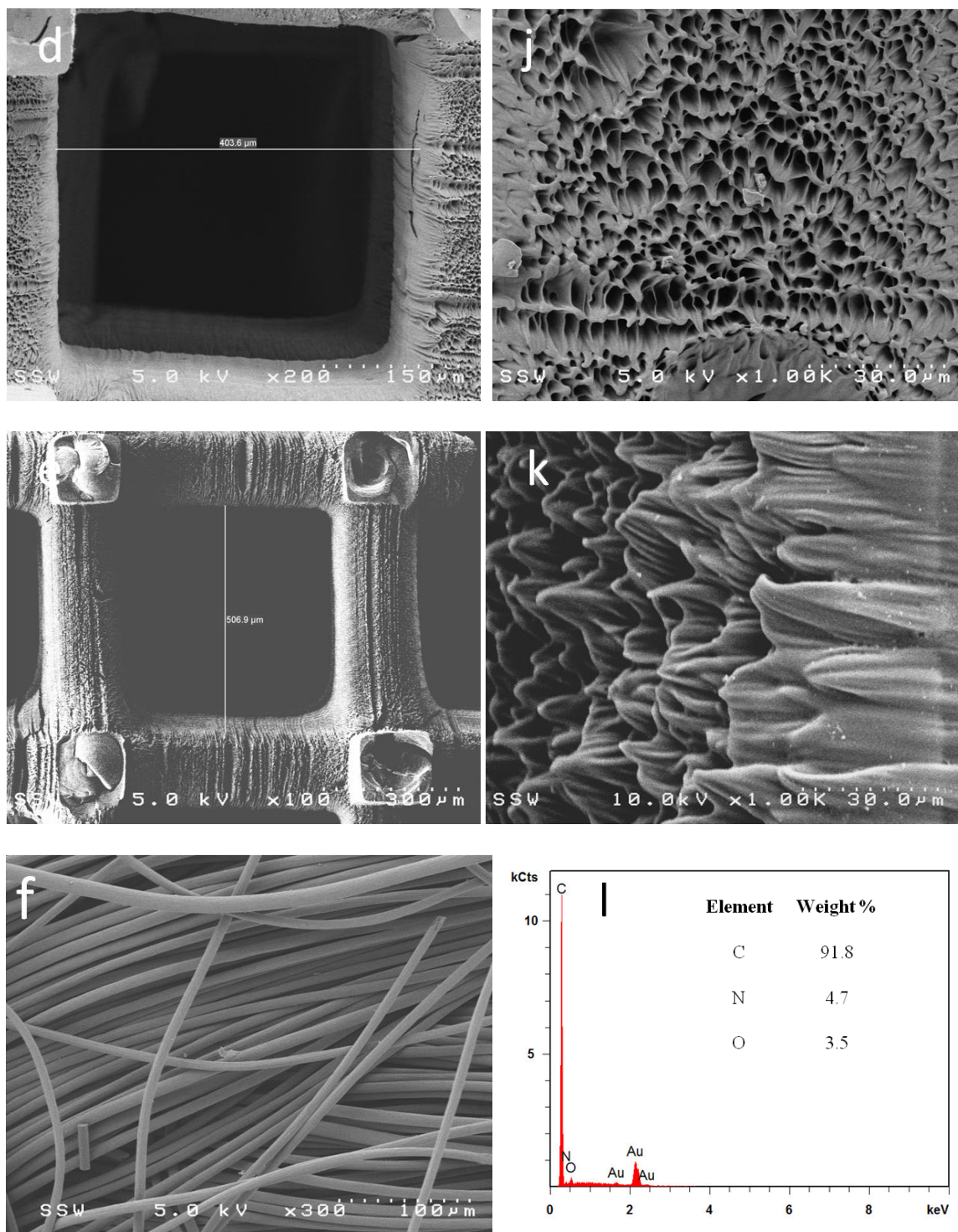
Figure 4.12: SEM images of well printed 3D porous anodes with pore sizes from 100 to 500 μm ((a) to (e)). (g)- (k) showed even smaller pores on 3D porous anode surface. (f) was carbon cloth surface and (l) presented EDX data of carbonized anodes.

In order to investigate the impact of porous structures on bacterial growth on MFC anodes, FESEM was further used to observe the biofilm formation on the six MFC anodes after 40 days of MFC operation. We found that the outer surface of both 3D printed carbon porous anodes and the carbon cloth anode was covered by thick layers of bacterial biofilm and extracellular polymeric substances (EPS) (Fig. 4.13 (f), (g)). Bacteria produce EPS to prompt cell attachment on anode surface, aggregation, and biofilm formation. EPS are composed of proteins, polysaccharides, nucleic acids, lipids and other biological macromolecules. The length of the MR-1 cells was several microns and EPS were generated to connect the bacterial cells. Apart from the biofilm on the top layers, MR-1 cell aggregation was also discovered on the inner layer surface of 3D printed porous anodes. Lots of long MR-1 cells were found growing and connecting with each other and EPS across the pores located at the internal anode surface. Nevertheless, few MR-1 cells were observed on the inner surface of the carbon cloth anode, indicating poor mass transport into the anode. This might be the reason why 3D printed carbon porous anodes generated higher electricity output compared to the carbon cloth anode. And since bacteria grown on outer porous layer had easier access to organism for food, there were slightly more bacteria adhering to outer porous layers than inner ones. However, the density of the bacterial cells was various due to the different pore sizes of the 3D anodes (Fig. 4.13 (a) - (e)). The inner surface of the 300 μm pore-sized anode was observed to have the highest bacterial cell density accumulated, while the 100 μm pore-sized anode had the lowest. This explains the much better performance, such as maximum cell voltage and power density, of MFCs with the 300 μm pore-sized anode. The low cell density on the 100 μm pore-sized anode might result from the poor mass

transfer from the medium into the internal layers. Bacterial biofilm on the inner layers of 400 μm and 500 μm pore-sized anodes were also pretty thick. However, large loopholes were observed in the biofilm on these two anodes, the size of which increased with the pore sizes of the anodes. As stated in Chapter 2, the power output of MFCs mainly depends on the electron transfer between anodes and bacterial biofilm. The loopholes in the biofilm might result in the slightly inferior electrochemical performance of MFCs based on the two anodes. So the MFC with 300 μm pore-sized anode were expected to have the best electrochemical performance.
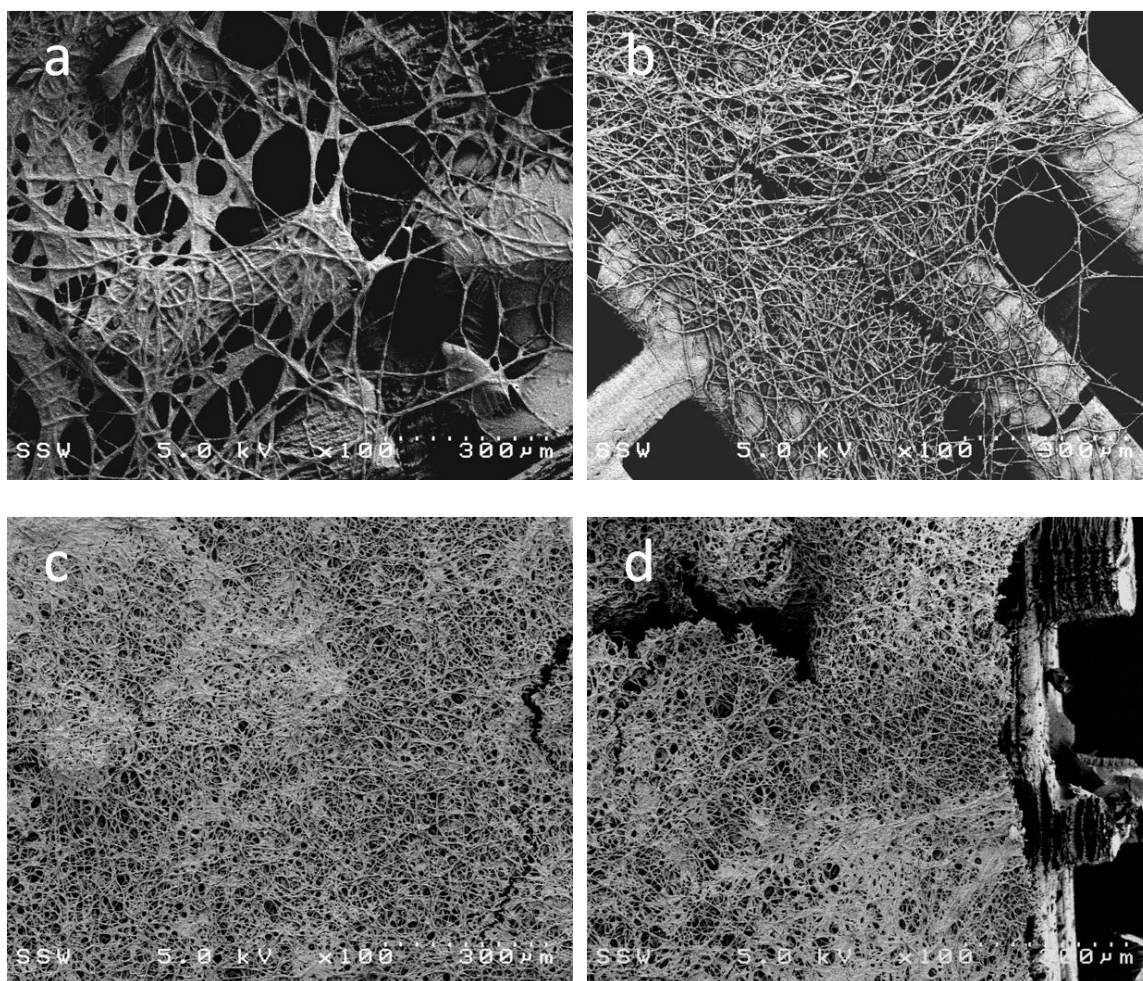
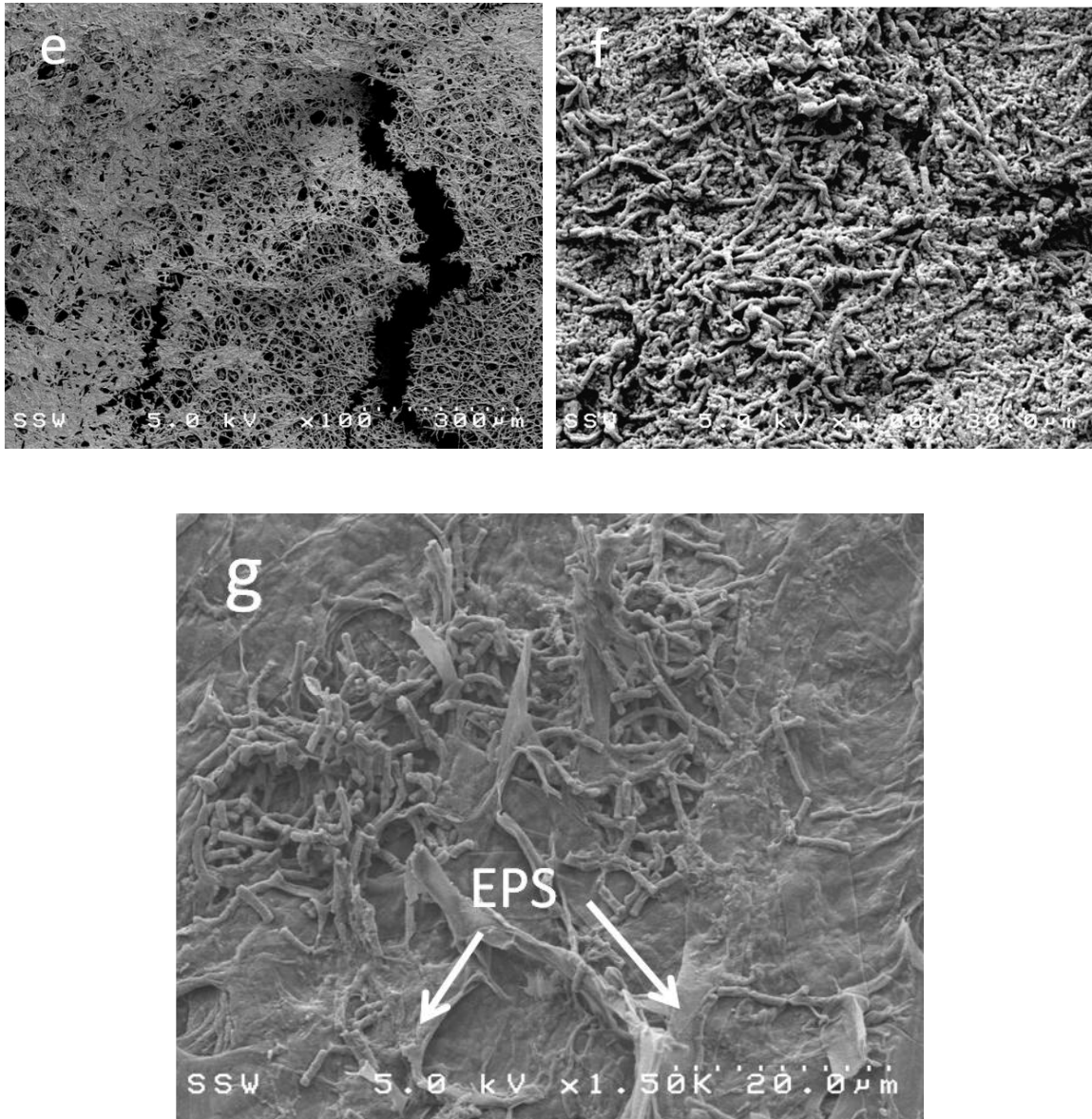**Figure 4.13: FESEM images of Shewanella MR-1 biofilm formed on the internal pore surface of 3D printed anodes ((a):100 μm, (b):200 μm, (c):300 μm, (d):400 μm, (e):500 μm), (f), (g) showed the biofilm formation on the outer surface of 3D printed porous anode and carbon cloth anode, respectively. Besides, extracellular polymeric substances (EPS) were observed in the sample.**

4.4 Conclusion

In this chapter, 3D printing technique was used to fabricate the 3D micro porous structures, followed by carbonization process. The 3D porous carbon structures with good conductivity served as novel anodes for air-cathode MFCs. The MFC with a 300 μm pore-sized anode achieved a maximum power density of $233.5mW/m^2$, which was 3.4-fold higher than that of the MFC with carbon cloth anode. The porous anodes afforded an open structure for bacterial adhesion and biofilm growth, enabling good mass transfer and internal bacterial colonization. The higher electricity output of all the five MFCs with 3D printed micro porous anodes also benefited from the higher surface area of anodes and good biocompatibility of carbon materials, which promoted active surface interaction with the bacterial biofilm and thus facilitated electron transfer from exoelectrogens to carbonized anodes. With the capacity of fabricating electrodes with tunable pore sizes, 3D printing technology provides a novel platform for high-performance MFC anode designing and preparation, which is promising for large-scale MFC application.

Chapter 5

5 Thesis Summary and Future Work

5.1 Summary

In this dissertation, three-dimensional printing technology was utilized to fabricate 3D porous structures, to serve as anodes in microbial fuel cells. Copper electroless plating and carbonization procedure were applied to the printed porous polymer matrixes to either enhance their conductivity or improve their biocompatibility. Several tests and characterization of MFCs based on different anode materials were conducted, in order to explore the properties and functions of 3D printed micro porous anodes and their excellent performance of the application in MFCs.

A brief introduction to MFCs and the mechanisms of extracellular electron transfer were reviewed and discussed in Chapter 2. The commonly used anode materials including carbonaceous, metal and metal oxide, and modified composite anode materials were also discussed in detail. The literature showed that increases in surface area of anodes would lead to the increase in power output of MFCs. Thus 3D printing technology was reviewed for its unique advantage in fabricating complicated and low cost structures and devices with precisely tunable and controllable pore sizes. The 3D printing method and its application in various fields (especially the potential usage in MFCs) were also presented.

Chapter 3 described the detailed procedures of 3D porous anode preparation, copper electroless plating and S. oneidensis MR-1 cultivation. MFCs with 3D copper porous

anode, copper mesh anode and carbon cloth anode were constructed and tested for comparison. A maximum voltage of 65.7±3mV and a maximum power density of 6.45±0.5 mWm^{-2} were achieved for MFCs with 3D copper porous anode while only 7.6±0.5mV and 0.53±0.04 mWm^{-2} were achieved for copper mesh anode, showing the great advantage of 3D porous anodes in MFCs compared to flat anode structures. However, a 3-fold larger maximum voltage and a ~10-fold higher power density were measured for MFCs with carbon cloth anode compared to 3D copper porous anode, indicating the possible copper corrosion during MFC operation. 732 µg/L copper ions were detected by ICP-MS confirming the copper corrosion in MFC medium. EDX analysis also demonstrated that copper content of the copper coating on 3D printed polymer matrix decreased due to corrosion. Biofilm on the anodes was characterized by SEM after 40 days operation and far less biofilm was observed on copper anodes compared to carbon cloth anode, illustrating copper coating wasn't suitable for MFC due to corrosion even though 3D micro porous structures were quite promising.

The unpleasant results in Chapter 3 forced the utilization of 3D printed carbon porous anodes in MFCs. In Chapter 4, the preparation processes of the 3D carbonized porous anodes with tunable pore sizes (ranging from 100 µm to 500 µm) were discussed in detail. Same bacterial cultivation and MFC operation procedures were used. The 3D printed carbon porous anodes exhibited much higher maximum voltages compared to the carbon cloth anode, especially the 300 µm pore-sized anode producing more than 2 times larger voltage than carbon cloth (453.1±8.5VS. 190±5). Higher power densities could also be measured for 3D carbon porous anodes indicating the overall better performance of MFCs with 3D porous anodes than that with carbon cloth anode. EIS was conducted to

further study the electrochemical properties of the six anode structures. The charge transfer resistance and the solution resistance total were quite similar for all the six anodes, but the diffusion resistance of the carbon cloth anode was about 3 times larger than the average diffusion resistance of 3D printed porous anodes, illustrating better mass transfer property of the porous structures. SEM was utilized to characterize the surface of the six anodes before and after MFC operation. Results showed that apart from micro porous structures, smaller pores with sizes of several microns were observed at the rods of the 3D printed porous anodes, enabling more bacterial adhesion and thicker bacterial biofilm formation afterward. The 3D printed carbon porous anodes were thus demonstrated to enhance the electricity output of MFCs.

5.2   Thesis Contributions

The contributions of this thesis are summarized below:

1) The first application of 3D printing technology in anode preparation for microbial fuel cells. The utilization of 3D printing technology in MFCs provides a promising solution to MFC scale-up as well as electricity output enhancement. As large scale anodes with controllable pore sizes could be prepared by 3D printing at a relative low cost, the MFC scale-up could be expected with the advance in 3D printing technology and material science, inspiring further investigations into practical approach to MFC scale-up.

2) 3D printed carbon porous anodes reported in this thesis demonstrated better electrochemical performances and excellent biocompatibility compared to carbon cloth anode, showing great potential of 3D porous anodes in MFCs. More

exploration into bacterial growth environment in 3D porous structures and methods of 3D porous anode fabrication will be encouraged, to further enhance the power output of MFCs

3) By exploring the carbonization procedures of 3D porous polymer structures, this thesis work opens up future opportunities of utilizing natural porous materials for MFC anode carbonization and thus develops an easy way of 3D carbon porous anode preparation.

4) This thesis also explored in depth the copper corrosion occurred during MFC operation, which further confirmed the toxic nature of copper to bacterial cells.

5.3 Future work

This thesis work has already demonstrated that the 3D printed micro porous carbon anodes for MFCs are reliable and have excellent performance. The properties of the anode materials and the performances of MFCs would be better if the following suggestions could be followed in future.

1) The carbonization process needs to be optimized. Although the current carbonization process is reliable to prepare 3D carbon porous anode with good conductivity, it also makes the carbonized structures rigid and fragile, which increases the difficulty of MFC construction.

2) Ways of larger size 3D printed anodes should be developed for future MFC scale-up. The current size of 3D printed porous anodes could reach about

15cm×15cm×75cm, which is large enough for experiment purpose. However, for large scale MFCs used to treat wastewater, the size above is far from enough.

3) Modification to the carbonized 3D porous structures has to be done to increase the conductivity of the materials. Though the carbonized structures share similar conductivity with the carbon cloth, they are far less conductive compared with metal coating.

Optimal pore sizes should be determined. Though the 300 μm pore-sized carbon anodes showed best performance in MFC application, more tests should be done to find the preferred pore sizes in different situations, in order to fulfill different requirements in various environments.

Appendices

Appendix A: Polarization curves for 3D printed carbon porous anodes.

a

b

c

d
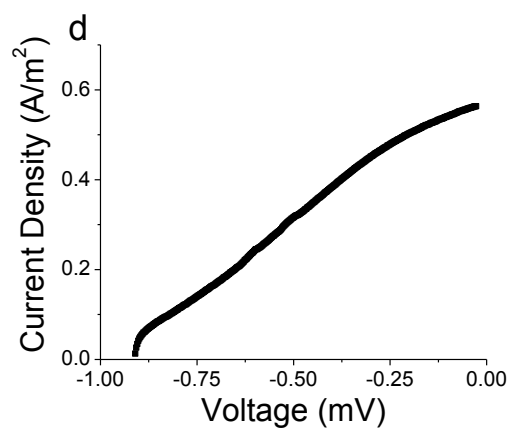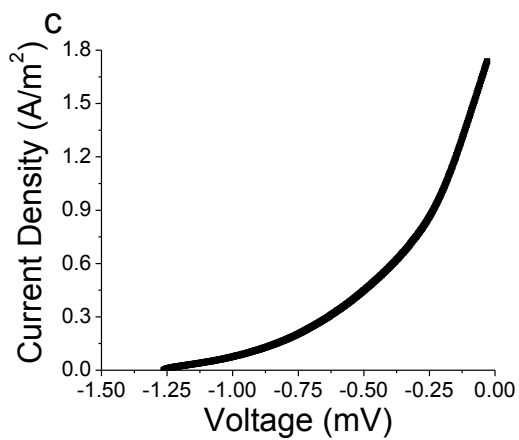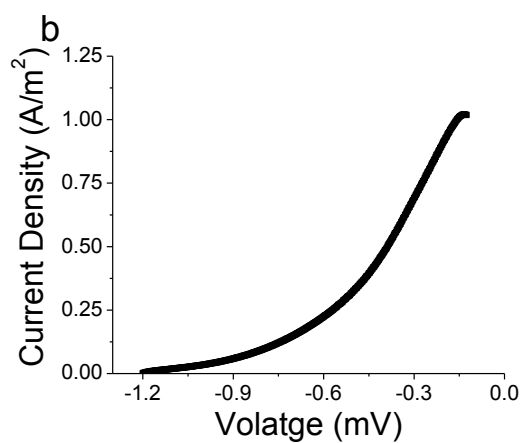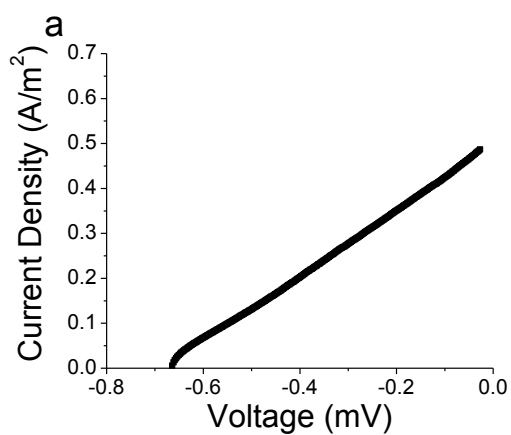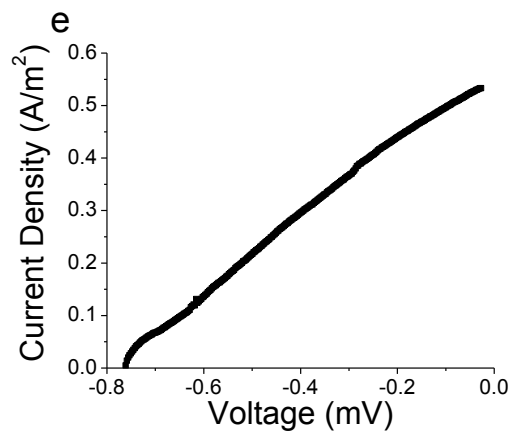
Appendix 1: Polarization curves for 3D printed carbon porous anodes (pore sizes ranging from 100 μm to 500 μm).

Appendix B: Bode plots of EIS measurement of MFCs with 3D printed carbon porous anodes and carbon cloth anode
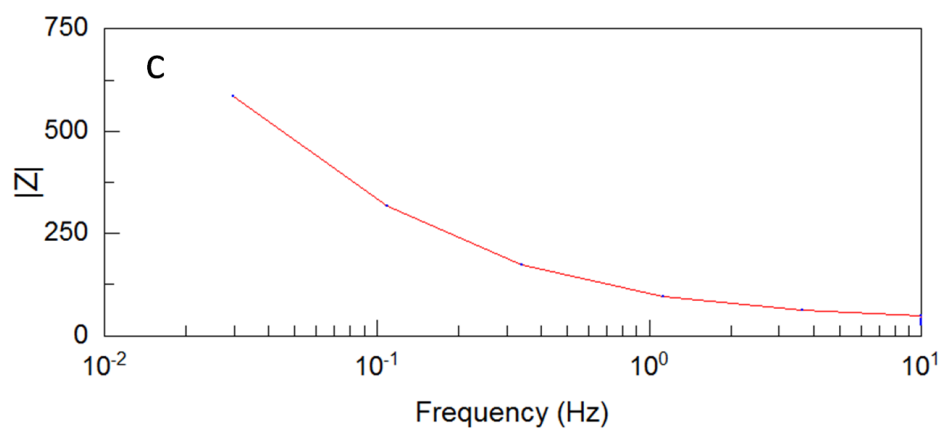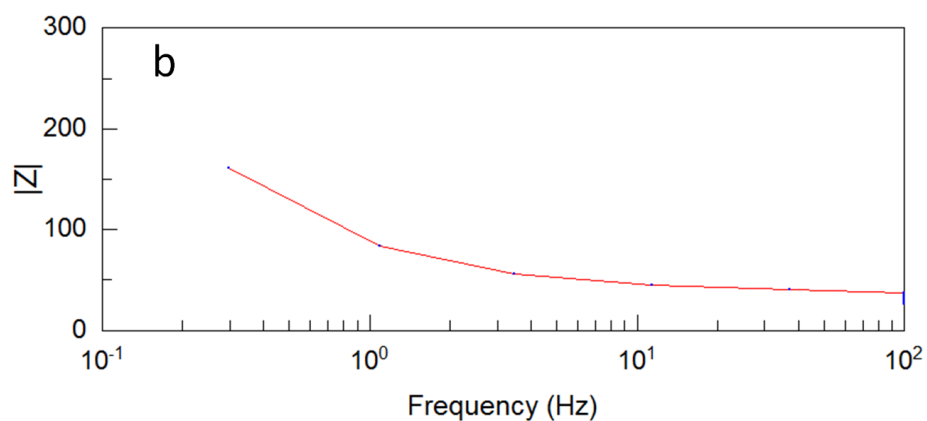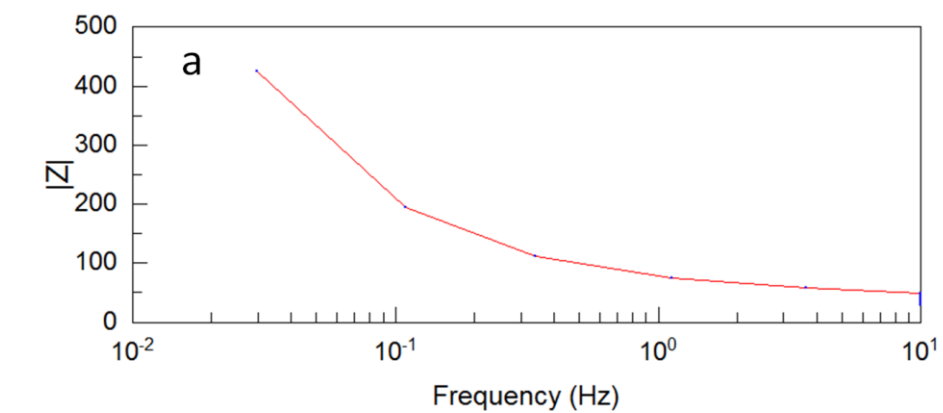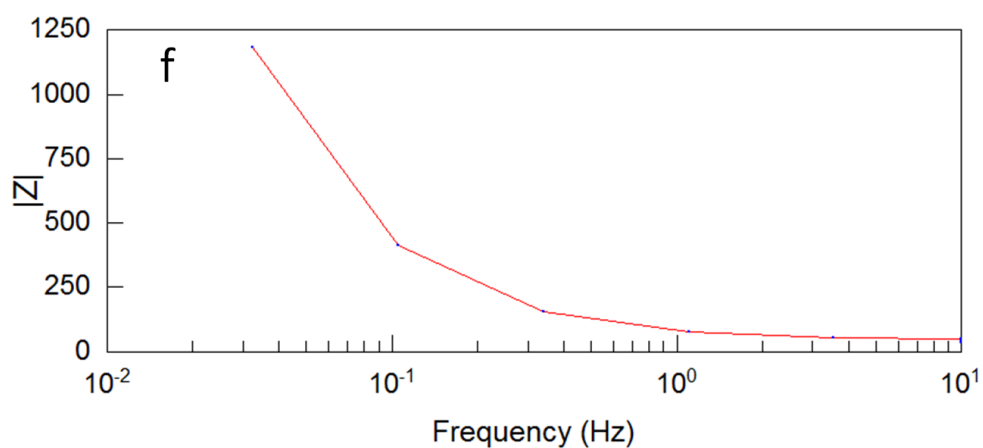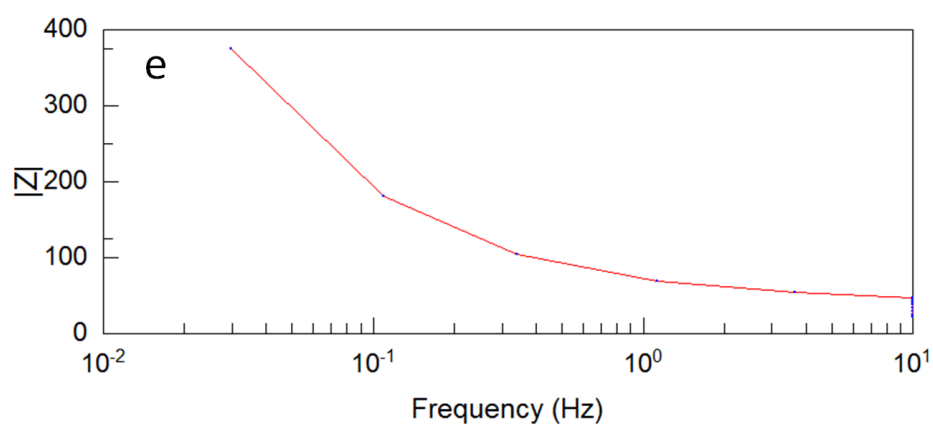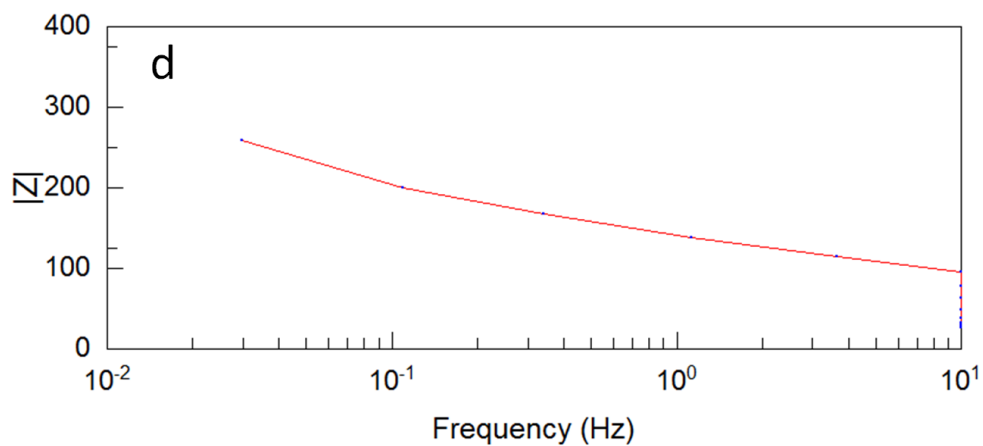
Appendix 2: Bode plots of EIS measurement of MFCs with 3D carbon porous anodes ((a)-(e): 100 μm-500 μm). (f) was the bode plot of carbon cloth anode.

References

1 World Water Council. 2011, Available from:

http://www.worldwatercouncil.org/index.php?id=25.

2 Logan B.E., Microbial Fuel Cell, 1st ed. John Wiley & Sons, Inc., Hoboken, 2007.

3 Xie X., Hu L., Pasta M., Wells G.F., Kong D., Criddle C.S., Cui Y., Nano Lett., 2010, 11, 291–296.

4 Yong Y.C., Dong X.C., Chan-Park M.B., Song H., Chen P., ACS Nano, 2012, 6, 2394–2400.

5 He Z., Liu J., Qiao Y., Li C.M., Tan T.T.Y., Nano Lett., 2012, 12, 4738–4741.

6 Xie X., Ye M., Hu L.B., Liu N., McDonough J.R., Chen W., Alshareef H.N., Criddle C.S., Cui Y., Energy Environ. Sci., 2012, 5, 5265-5270.

7 Wang X.L., Guo Q.Q., Cai X.B., Zhou S.L., Kobe B., Yang J., ACS Appl. Mater. Interfaces, 2014, 6 (4), 2583–2587.

8 Wang X.L., Cai X.B., Guo Q.Q., Zhang T.Y., Kobe B., Yang J., Chem. Commun., 2013, 49, 10064-10066.

9 Kar M.L., Greg W., Mohamed E.N., Yuri G., Gordon S., Woon M.L. and Jun Y., Nano Letters, 2013, 13, 2407–2411.

10 Potter M.C. Proc. R. Soc. Lond., B,1911, 84, 2760 -2761.

11 Qiao Y., Bao S.J., Li C.M., Cui X.Q., Lu Z.S., Guo J., ACS Nano, 2008, 2, 113-119.

12 Time. The 50 Best Inventions of 2009. Available online:

http://content.time.com/time/specials/packages/article/0,28804,1934027_1934003_19339 65,00.html

13 Reimers C.E., Tender L.M., Fertig S. and Wang W., Environ. Sci. Technol., 2001, 35, 192-195.

14 Davis F. and Higson S.P., J. Biosens. Bioelectron., 2007, 22, 1224-1235.

15 Logan B.E., Environ. Sci. Technol., 2004, 38, 160A-167A.

16 Logan B.E., Aelterman P., Hamelers B., Rozendal R., Schroder U., Keller J., Freguiac S., Verstraete W. and Rabaey K., Environ. ScL Technol., 2006, 40, 5181-5192.

17 Kim H.J., Hyun M.S., Chang I.S., et al. Microbiol. Biotechnol., 1999, 3, 365-367.

18 Kim B.H., Chang I.S., Gil G.C., Park H.S., Kim H.J., Biotechno. Lett., 2003, 25, 541-545.

19 Chaudhuri S.K. and Lovley D.R., Nat. Biotechnol., 2003, 21, 1229-1232.

20 Zhu B., Bai X.Y., Chen G.X., Yi W.M. and Bursell M., Int. J. Engine Res., 2002, 26, 57-66.

21 Liu H., Logan B.E., Environ. Sci. Technol., 2004, 38, 4040-4046.

22 Heidelberg J.F., Paulsen I.T., Nelson K.E., et al. Nat. Biotechnol., 2002, 20, 1118-1123.

23 Methe B.A., Nelson K.E., Eisen J.A., et al. Science, 2003, 302, 1967-1969.

24 Shi L., Squier T.C., Zachara J.M. and Fredrickson J.K. Molecular Microbiol., 2007, 65, 12-20.

25 Antonio R., Barbara M., Virgilio G., Silvia L., Paolo D.N. and Enrico T., Energy Environ. Sci., 2008, 1, 417–429.

26 Leung K.M., Wanger G., Naggar M.Y., Gorby Y., Southam G., Lau W.M. and Yang J., Nano Letters, 2013, 13, 2407–2411.

27 Reguera G., McCarthy K.D., Mehta T., Nicoll J.S., Tuominen M.T. and Lovley D.R., Nature, 2005, 435,1098-1101.

28 Dewan A., Beyenal H., Lewandowski Z., Environ. Sci. Technol., 2008, 42, 7643–7648.

29 Rabaey K., Clauwaert P., Aelterman P., Verstraete W., Environ. Sci. Technol. 2005, 39, 8077–8082.

30 Aelterman P., Versichele M., Marzorati M., Boon N., Verstraete W., Bioresour. Technol., 2008, 99, 8895–8902.

31 Rezaei F., Richard T.L., Brennan R.A., Logan B.E., Environ. Sci. Technol., 2007, 41, 4053–4058.

32 Wang X., Cheng S.A., Feng Y.J., Merrill M.D., Saito T., Logan B.E., Environ. Sci. Technol., 2009, 43, 6870–6874.

33 Logan B.E., Cheng S.A., Watson V., Estadt G., Environ. Sci. Technol., 2007, 41, 3341–3346.

34 He Z., Minteer S.D., Angenent L.T., Environ. Sci. Technol., 2005, 39, 5262–5267.

35 Wei J., Liang P., Huang X., Bioresource Technology, 2011,102, 9335–9344.

36 Chen S.L., Hou H.Q., Harnisch F., Patil S.A., Martinez A.C., Agarwal S., Zhang Y.Y., Ray S.S., Yarin A.L., Greiner A., Schroder U., Energy & Environ. Sci., 2011, 4, 1417-1421.

37 Xie X., Yu G.H., Liu N., Bao Z.N., Criddle C.S., Cui Y., Energy & Environ. Sci., 2012, 5, 6862-6866.

38 Karra U., Manickam S.S., McCutcheon J.R., Patel N., Li B., Int. J. Hydrogen Energy, 2013, 38, 1588-1597.

39 Manickam S.S., Karra U., Huang L.W., Bui N.N, Li B.K., McCutcheon J.R., Carbon, 2013, 53, 19-28.

40 Dumas C., Basseguy R., Bergel A., Electrochim. Acta, 2008a, 53, 5235-5241.

41 Wang H., Wang G., Ling Y., Qian F., Song Y., Lu X., Chen S., Tong Y., Li Y., Nanoscale, 2013, 5, 10283-10290.

42 Richter H., McCarthy K., Nevin K.P., Johnson J.P., Rotello V.M., Lovley D.R., Langmuir, 2008, 24, 4376-4379.

43 Schroder U., NieBen J. and Scholz F.A., Chem. Int. Ed, 2003, 42, 2880-2883.

44 Tang J., Yuan Y., Liu T., Zhou S., J. of Power Sources, 2015, 274, 170-176.

45 Zhang C., Liang P., Jiang Y., Huang X., J. of Power Sources, 2015, 273, 580-583.

46 Lv Z., Xie D., Li F., Hu Y., Wei C., Feng C., J. of Power Sources, 2014, 246, 642-649.

47 Zhang L.L., Zhao X.S., Chem. Soc. Rev., 2009, 38, 2520-2531.

48 Jiang J., Li Y.Y., Liu J.P., Huang X.T., Yuan C.Z., Lou X.W., Adv. Mater., 2012, 24, 5166-5180.

49 Lv Z.S., Xie D.H., Yue X.J., Feng C.H., Wei C.H., J. of Power Sources, 2012, 210, 26-31.

50 Feng Y.J., Yang Q., Wang X., Logan B.E., J. of Power Sources, 2010, 195(7), 1841-1844.

51 Saito T., Mehanna M., Wang X., Cusick R.D., Feng Y.J., Hickner M.A., Logan B.E., Biores. Technol., 2011, 102(1), 395-398.

52 Zhou M.H., Chi M.L., Wang H.Y., Jin T., Biochem. Engineer. J., 2012, 60, 151-155.

53 Tang X.H., Guo K., Li H.R., Du Z., Tian J., Bioresource Technology, 2011, 102(3), 3558-3560.

54 Liu J., Liu J.F., He W.H., Qu Y.P., Ren N.Q., Feng Y.J., J. of Power Sources, 2014, 265, 391-396.

55 Peng L., You S.J., Wang J.Y., Biosensors & Bioelectronics, 2009, 25(5), 1248-1251.

56 Xie X., Hu L.B., Pasta M., Wells G.F., Kong D.S., Criddle C.S., Cui Y., Nano Letters, 2011, 11(1), 291-296.

57 Zhang Y., Mo G., Li X., Zhang W., Zhang J., Ye J., Huang X. and Yu C., J. of Power Sources, 2011, 196, 5402-5407.

58 Huang Y.X., Liu X.W., Xie J.F., Sheng G.P., Wang G.Y., Zhang Y.Y., Xu A.W., Yu H.Q., Chem. Commun. 2011, 47, 5795-5797.

59 Qiao Y., Bao S.J., Li C.M., Cui X.Q., Lu Z.S. and Guo J. ACS nano, 2007, 2, 113-119.

60 Chen H., Yong Y.C., Kim D.H. and Song H., Chem. Commun. 2011, 47, 12825-12827.

61 Qiao Y., Li C.M., Bao S.J., Bao Q.L., J. of Power Sources, 2007, 170(1), 79-84.

62 Zou Y.J., Xiang C.L., Yang L.N., Sun L.X., Xu F., Cao Z., Int. J. Hydrogen Energy, 2008, 33(18), 4856-4862.

63 SPIE-Professional. Chuck Hull: Pioneer in tereolithography.

http://spie.org/x91418.xml (accessed September 27, 2013).

64 3D Systems. 30 Years of Innovation. http://www.3dsystems.com/ (accessed September 27, 2013).

65 Sachs E.M., Haggerty J.S., Cima M.J., Williams P.A., Three dimensional printing techniques. U.S. 1993 Patent 5, 204, 055.

66 Jones R., Haufe P., Sells E., Iravani P., Olliver V., Palmer C., Bowyer A., Robotica 2011, 29, 177−191.

67 Leukers B., Gülkan H., Irsen S.H., Milz S., Tille C., Schieker M., Seitz H.J., Mater. Sci. Mater. Med., 2005, 16, 1121−1124.

68 Mironov V., Boland T., Trusk T., Forgacs G., Markwald R.R., Trends Biotechnol., 2003, 21, 157−161.

69 Lipton J., Arnold D., Nigl F., Lopez N., Cohen D., Noren N., Lipson H., In Solid Freeform Fabrication Symposium, 2010.

70 Daanen H., Hong S.A., Int. J. Cloth. Sci. Technol., 2008, 20, 15−25.

71 Campbell J., Parsons J., J. Text. Apparel, Technol. Manage., 2005, 4, 1−10.

72 Hull C.W., Apparatus for production of three-dimensional objects by stereolithography. 1986, U.S. Patent 4, 575, 330.

73 Melchels F.P.W., Feijen J., Grijpma D.W., Biomaterials, 2010, 31, 6121−6130.

74 Pan Y., Zhou C., Chen Y., In Proceedings of the 2012 International Manufacturing Science and Engineering Conference, 2012, pp 4−8.

75 Bethany C.G., Jayda L.E., Sarah Y.Lo., Chen C., and Dana M.S., Anal. Chem., 2014, 86, 3240−3253.

76 Cooke M. N., Fisher J.P., Dean D., Rimnac C., Mikos A.G., J. Biomed. Mater. Res., Part B: Appl. Biomater., 2003, 64, 65−69.

77 Huang Y.M., Kuriyama S., Jiang C.P., Int. J. Adv. Manuf. Technol., 2004, 24, 361−369.

78 FormLabs. Formlabs-High Resolution Desktop 3D Printer. http://formlabs.com/ (accessed September 30, 2013).

79 Beaman J.J., Deckard C.R., Selective laser sintering with assisted powder handling. U.S. 1990, Patent 4, 938, 816.

80 Kumar S., JOM, 2003, 55, 43−47.

81 Yan X., Gu P., Comput.-Aided Des., 1996, 28, 307−318.

82 Ko S.H., Pan H., Grigoropoulos C.P. Luscombe C.K., Fréchet J.M.J., Poulikakos D., Nanotechnology, 2007, 18, 345202.

83 Ziemian C.W., Crawn P.M., III Rapid Prototyp. J., 2001, 7, 138−147.

84 Yang Y.Q., Shanghai Packaging, 2015, 4, 64-65.

85 Gross D. Texas company makes metal gun with 3-D printer. CNN. Retrieved 9 November 2013.

86 Simon J.L., Robert J.B., Christopher P.P., Duncan R.B., David A.H, PLOS ONE, 2012, 7, 11, 49365

87 Hedges M., Marin A.B., Originally presented at DDMC 2012 Conference, 14-15, 3, 12, Berlin.

88 C. Lee Ventola MS, P&T Community, 2014, 39, 10, 704-711.

89 McKinsey Global Institute, 2013. Disruptive Technologies: Advances That Will Transform Life, Business and the Global Economy. McKinsey Global Institute & Company, Seoul/South Korea.

90 Reeves, 2013. 3D Printing in Aerospace and Automotive.Econolyst Ltd., Derbyshire, UK

91 Malte G., Anton J.M., Schoot U., Cindy V., Energy Policy, Article in press.

92 Wurtz A., Hebd C.R., Acad. Sci., 1844, 18, 702–704.

93 Brenner A., Riddell G., J. Res. Nat. Bur. Stand, 1946, 37, 31–34.

94 Brenner A., Riddell G., J. Res. Nat. Bur. Stand, 1947, 39, 385–395.

95 Zhang T.Y., Wang X.L., Li T.J., Guo Q.Q. and Yang J., J. Mater. Chem. C., 2014, 2, 286-294.

96 Shacham-Diamand Y., Osaka T., Datta M., Ohba T., Advanced ULSI. Interconnects: Fundamentals and Applications, Springer, 2009.

97 Murarka S.P., Verner I.V., Gutmann R.J., Copper-Fundamental Mechanisms for Microelectronic Applications, John Wiley and Sons, New York, 2000.

98 Bretschger O., Obraztsova A., Sturm C.A., Chang I.S., Gorby Y.A., et. al., Appl. Environ. Microbiol., 2007, 73(21), 7003–7012.

99 Goldstein J., Scanning Electron Microscopy and X-Ray Microanalysis, Springer, 2003. Retrieved 26 May 2012.

100 Wolfgang M., van Putten J.P.M., Hayes S.F., Dorward D. and Koomey M., Embo Journal, 2000, 19, 6408-6418.

101 El-Naggar M.Y., Wanger G., Leung K.M., Yuzvinsky T.D., Southam G., Yang J., Lau W.M., Nealson K.H. and Gorby Y., PNAS, 2010,107, 18127-18131.

102 Zhu X., Logan B.E., J. Chem. Technol. Biotechnol., 2014, 89, 471–474.

103 Hoogers G., Ed. Fuel Cell Technology Handbook, CRC Press: Boca Raton, FL, 2003.

104 Newton G.J., Mori S., Nakamura R., Hashimoto K., and Watanabe1 K., Appl. Environ. Microbol., 2009, 75, 7674–7681.

105 Sazanov Yu.N., Gribanov A.V. and Lysenko V.A., Fibre Chemistry, 2008, 40, 4, 355-364.

106 Artem'ev V.B., Eremin I.V., et al., Nedra Communications Ltd, Moscow, 1999.

107 Gyul'maliev A.M., Golovin G.S. and Gladun T.G., Theoretical Principles of Coal Chemistry, MGGU, Moscow, 2003.

108 Chen X., Li C., Gratzel M., Kostecki R. and Mao S. S., Chem. Soc. Rev., 2012, 41, 7909–7937.

109 Arico A.S., Bruce P., Scrosati B., Tarascon J.M. and Van Schalkwijk W., Nat. Mater., 2005, 4, 366–377.

110 Li W.W., Yu H.Q. and He Z., Energy Environ. Sci., 2014, 7, 911–924.

111 Zhang L. L. and Zhao X. S., Chem. Soc. Rev., 2009, 38, 2520–2531.

112 Mhamane D., Suryawanshi A., Unni S.M., Rode C., Kurungot S. and Ogale S., Small, 2013, 9, 2801–2809.

113 Yadav P., Banerjee A., Unni S., Jog J., Kurungot S. and Ogale S., ChemSusChem, 2012, 5, 2159–2164.

114 Zhong M., Kim E.K., McGann J.P., Chun S.E., Whitacre J.F., Jaroniec M., Matyjaszewski K. and Kowalewski T., J. Am. Chem. Soc., 2012, 134, 14846–14857.

115 Jiang H., Lee P.S. and Li C., Energy Environ. Sci., 2013, 6, 41–53.

116 Coats A.W. and Redfern J.P., Analyst, 1963, 88, 906-924.

117 Alexander C., Sadiku M., Fundamentals of Electric Circuits (3, revised ed.), McGraw-Hill, 2006, 387–389.

118 Watson V.J., Logan B.E., Biotechnology and Bioengineering, 2010, 105, 3, 489-498.

119 Wei B., Tokash J.C., Zhang F., Kim Y., Logan B.E., Electrochimica Acta, 2013, 89, 45–51.

120 He Z. and Mansfeld F., Energy Environ. Sci., 2009, 2, 215–219.

121 Wang Y., Shao Y., Matson D.W., Li J., Lin Y., ACS Nano, 2010, 4, 1790-1798.

122 Jia L., Wang D.H., Huang Y.X., Xu A.W., Yu H.Q., J. Phys. Chem. C, 2011, 115, 11466-11473.

Curriculum Vitae

Name: Bin Bian

Post-secondary   Southeast University
Education and   Nanjing, Jiangsu Province, China
Degrees: 2009-2013 Bachelor of Engineering Science

                         The University of Western Ontario
                         London, Ontario, Canada
                         2013-2015 Master of Engineering Science

Honours and   National Encouragement Scholarship
Awards: 2010-2011, 2011-2012

                         Guanghua Scholarship
                         2012-2013

                         Western Graduate Research Scholarship
                         2013-2015

Related Work   Research/Teaching Assistant
Experience   The University of Western Ontario
                         2013-2015

Publications:

1. Bin Bian, Mingjun Hu, Zhaoliang Yang, Xiaobing Cai, Jun Yang. 3D printed porous anode with copper coating impacts power output in microbial fuel cells, *RSC Advances* (submitted)

2. Mingjun Hu, Xiaobing Cai, Qiuquan Guo, Bin Bian, Tengyuan Zhang, Jun Yang. Direct pen writing of adhesive particle-free ultrahigh silver salt-loaded composite ink for stretchable circuits, *Advanced Electronics Materials* (submitted)

3. Naibo Zhang, Mingjun Hu, Bin Bian, and Jun Yang. Design and Fabricate Quadrifilar Helix Antenna Based on 3D Printing Technology, *Electronics Letters* (submitted)